Widespread erroneous analysis of the Fe 2p peak in X-ray photoelectron spectroscopy examination in corrosion studies

Hughes, Anthony E.; Easton, Christopher D.; Anusuyadevi, Prasaanth Ravi; Raeber, Thomas J.; Wilson, Nick C.; Mol, Arjan

DOI
10.1016/j.corsci.2025.113357

Publication date
2025

Document Version
Final published version

Published in
Corrosion Science

Citation (APA)
Hughes, A. E., Easton, C. D., Anusuyadevi, P. R., Raeber, T. J., Wilson, N. C., & Mol, A. (2025). Widespread erroneous analysis of the Fe 2p peak in X-ray photoelectron spectroscopy examination in corrosion studies. *Corrosion Science*, *257*, Article 113357. https://doi.org/10.1016/j.corsci.2025.113357

Corrosion Science 257 (2025) 113357

Contents lists available at ScienceDirect

Corrosion Science

journal homepage: www.elsevier.com/locate/corsci

Widespread erroneous analysis of the Fe 2p peak in X-ray photoelectron spectroscopy examination in corrosion studies

Anthony E. Hughes [a,b,*], Christopher D. Easton [c], Prasaanth Ravi Anusuyadevi [d], Thomas J. Raeber [c], Nick C. Wilson [a], Arjan Mol [d,**]

[a] CSIRO Mineral Resources, Gate 5, Normanby Rd, Notting Hill, Victoria 3169, Australia
[b] Institute for Frontier Materials, Deakin University, 75 Pigdons Rd, Waurn Ponds, Geelong, Victoria 3216, Australia
[c] CSIRO Manufacturing, Gate 3, Normanby Rd, Notting Hill, Victoria 3169, Australia
[d] Department of Materials Science and Engineering (MSE), Faculty of Mechnical Engineering (ME) Delft University of Technology, Mekelweg 2, Delft 2628CD, the Netherlands

ARTICLE INFO

Keywords:
Corrosion
XPS
Iron
Ion-oxides
Curve fitting

ABSTRACT

XPS analysis is routinely used in corrosion studies to analyse corrosion product and protective layers on a range of metals. In the case of transition metals and especially iron, the extraction of information about chemical species including identification and quantification requires complex fitting of the metal 2p spectrum. Unfortunately, there is extensive misunderstanding of what is required for fitting of these metal 2p photoelectron peaks. In the case of high spin Fe 2p compounds there is a complex structure based on multiplet and satellite peaks which is often ignored. In this review of the application of XPS in the study of corrosion and protection of ferrous metals; we quantify the extent of misinterpretation of XPS Fe 2p spectra within the literature. It is found that in over 70 % of papers there is an adamant misunderstanding of the requirements for fitting Fe 2p, which can be divided into three groups. First, in the most serious case, there seems to be a lack of understanding of spin orbit coupling which gives rise to the major Fe $2p_{3/2}$ and Fe $2p_{1/2}$ peaks with the latter being incorrectly assigned to a different chemical species. Second, satellite structures are often assigned to a different chemical species. Third, single peaks are used to fit chemical components whereas a complex multiplet structure should be employed. We establish the extent to which these errors are made by critical appraisal of over 220 papers published in selected years between 2015 and 2024.

1. Introduction

X-ray Photoelectron Spectroscopy (XPS) is often used in the characterisation of surface coatings and corrosion product for various irons, steels and other ferrous metals. However much of this characterisation has been poorly performed leading to erroneous interpretation of XPS spectra, particularly the Fe 2p analysis. Embodied in the literature is a widespread lack of understanding of the basic physics of photoelectron emission meaning that incorrect approaches to curvefitting of the Fe 2p has become the norm. This paper explores the reasons why this situation has arisen and provides direction on the better approaches for Fe 2p analysis.

Typically, XPS is used to identify chemical species, oxidation states and to perform (semi-)quantitative analysis. In many cases XPS is relatively straight forward to perform and interpret. For example, in cases such as the light metals, chemical states can be obtained from the peak positions and composition from the peak areas. There are well prepared guides for this type of analysis [1]. If more than one oxidation state is present, then fitting symmetric peaks to spectral envelopes usually suffices to extract the information relating to those different oxidation states. The authors refer to this approach as *chemistry* fitting [2].

What is often hidden and therefore overlooked, in these examples of XPS spectral analysis, is the complex underlying physics of X-ray induced photoelectron emission based on quantum mechanics (QM). This complexity becomes apparent when examining transition metals or the rare earths where spectral features cannot be simply fitted by using a single peak to represent a single oxidation state or chemical species [3,

* Corresponding author at: CSIRO Mineral Resources, Gate 5, Normanby Rd, Notting Hill, Victoria 3169, Australia
** Corresponding author.
E-mail addresses: Tony.Hughes@csiro.au (A.E. Hughes), J.M.C.Mol@tudelft.nl (A. Mol).

https://doi.org/10.1016/j.corsci.2025.113357
Received 17 July 2025; Received in revised form 22 September 2025; Accepted 24 September 2025
Available online 26 September 2025

4]. Recent theoretical studies examine in detail how the intensity under the Fe 2p peaks for certain oxides is spread over a broad range of Binding Energies (BEs) in literally thousands of multiplet peaks [5]. The reasons for this will be explored in more detail in the next section. Of course, fitting so many peaks to the Fe 2p envelope is not practical. An intermediate method between a full theoretical approach and fitting single peaks is to fit a limited number of peaks to reproduce the envelope of the Fe 2p spectrum and use these fits to obtain percentages of each type of oxide. This is called *envelope* fitting. A recent study of this approach scoped out the limits of applicability of this approach to mixtures of oxides [2].

A related study [6] examined fitting of the Fe 2p region in austenitic stainless steels and found a relatively poor understanding of the task at hand since most studies adopted a chemistry approach to fitting thereby associating single symmetric peaks to individual oxidation states. This type of incorrect approach inevitably leads to significant errors in reported compositional analyses undermining any conclusions based on those analyses. This further emphasises the emergence of the "reproducibility crisis" in the XPS literature as highlighted by Linford et al. [7].

To emphasize the differences in these two approaches, "envelope" and "chemistry" fitting are depicted and explained in Fig. 1. Here FeO and Fe_2O_3 have been chosen because they are pure Fe^{2+} and Fe^{3+} respectively, i.e. there is no mixed oxidation state. As previously mentioned, the envelope approach based on the multiplet structures accurately reproduces the actual data (there is essentially no difference between the two). On the other hand, attempting to fit these data with

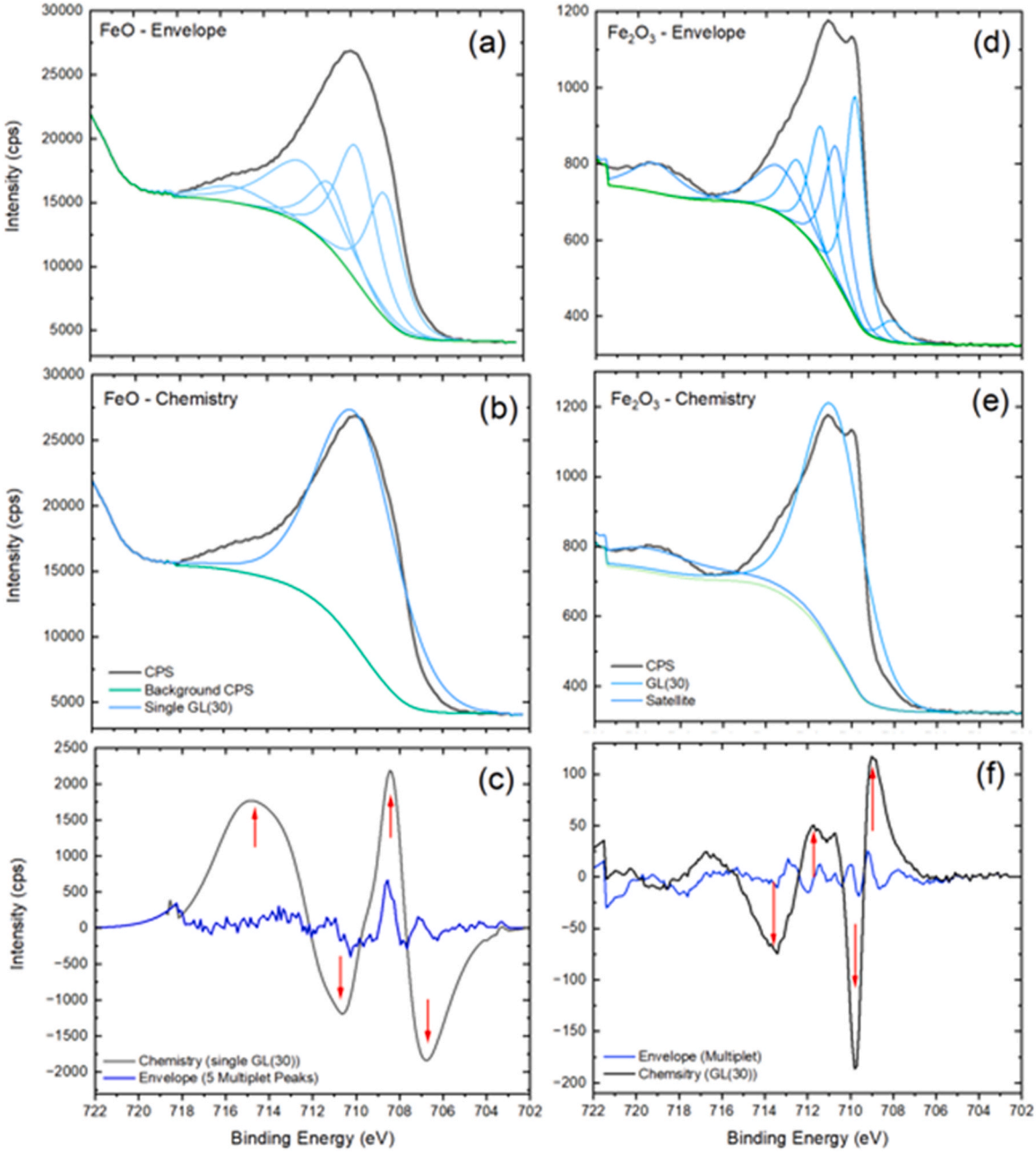

Fig. 1. Examples of fitting FeO and Fe_2O_3 with single peaks (chemistry) and multiplet peaks (envelope). (a) to (c): FeO and (d) to (f): Fe_2O_3. All multiplet structures are those reported in [2]. (a) envelope and (b) chemistry fits to FeO. (c) residuals between the data and the sum of the fits. (d) envelope and (e) chemistry fits to Fe_2O_3. (f) residuals between the data and the sum of the fits. All fits use a Shirely background. The fits in (b) and (e) are Gauss/Lorentz(30) peaks shapes. In (e), a satellite peak has been added as a second component in order to do the fitting over the same energy width. It was found that reducing the upper bound to 716.5 eV and only using one peak made < 1 % difference in the final peak parameter values.

single peaks leads to serious under/over estimation of the spectral data as seen for FeO and Fe_2O_3 in Fig. 1(b) and (e) respectively. This is clearly seen in their respective residuals in Fig. 1(c) and (f). Here the red arrows highlight the over/under estimation which is significantly higher than the envelope fitting (blue lines). The size of the excursions from the zero line (exact fitting) is such that the fits are statistically insignificant. This point was made in a previous paper by the authors [2] where it was shown that chemistry fitting was unable to recover the correct composition of mixtures of oxides.

The current paper extends the recent review on the application of XPS to the austenitic stainless steel [6] to the XPS of ferrous metals more generally found in corrosion studies. As shown below, there are well over a thousand such papers published since 2011; a landmark year defined by the publication of a paper by Biesinger et al. [8] who outlined a fitting procedure based on the known multiplet structure of the time. The procedure offered the promise of much better quantitative analyses than approaches that were used up to that time. More recently, it has been demonstrated that the Biesinger's envelope fitting approach can be used to determine quantitative results under a range of conditions; an outcome which cannot be achieved using the chemistry fitting approach [2]. This review, therefore, focuses on the extent to which the use of envelope fitting has been adopted amongst those reporting XPS of ferrous metals compared to the incorrect chemistry fitting approach.

2. Quantum mechanics background and multiplets

In 2025, the International Year of Quantum Science and Technology, it is worth focusing some attention on the QM origin of multiplets structures in XPS. By doing so we can attempt to correct the poor practice in XPS which ignores the underlying QM theory that explains XPS multiplets and other spectral features. We examine the origin of the QM model of the atom and how this model gives rise to multiplet structures.

In the early part of the 20th century, the group of Niels Bohr, first proposed a theoretical basis for the current quantum mechanical (QM) model of atoms *i.e.* that electrons populate discrete shells around a central nucleus. In the following years Wolfgang Pauli completed the QM model through the introduction of electron angular momentum (spin). This model provided an explanation for discrete lines observed in optical spectra which had been a puzzle in the latter part of the 19th century and early 20th century. The QM explanation of the optical bands was as follows: electrons in atoms had fixed, discrete electron orbitals and transitions between these orbitals, governed by QM rules, result in photon emission (or absorption) and are also discrete explaining the observed sets of lines in optical emission spectra instead of a continuous spectrum that would be expected based on classical concepts. It also explained the chemical basis of the arrangement of elements in the periodic table of the elements.

The orbitals themselves are characterised by quantum numbers, with the first four being quantum numbers, n, l, m_l and m_s [9]. The principal quantum number n designates the shell numbers of the orbital and is given by the natural numbers (1, 2, 3,…). These are split into subshells by the azimuthal quantum number l, given by the whole numbers (0, 1, 2….) but are often referred to as s, p, d, f (derived from the appearance of spectral lines in alkali metals). Additional quantum numbers m_l and m_s were added to account for the quantised angular momenta and magnetic moments of the electron orbits and the spin angular momentum. The azimuthal momenta and magnetic moments are coupled, therefore the number of values that m_l can adopt is dependent on l and has $2\,l+1$ values, so that the s subshell has one orbital, the p subshell has three orbitals and so on. The spin magnetic quantum number, m_s was added to explain splitting of optical lines observed under an applied magnetic field – the Zeeman effect. This quantum number is referred to today as the spin vector of the electron: it can only adopt two values namely $\pm$ ½.

The corollary of the above paragraphs is that distinct spectral lines in optical emission spectra led to the development of a QM theory to describe the internal structure of atoms. The energies of these lines depended on the principal quantum number n, with further splitting of these energies dictated by all other quantum numbers. As no two bound electrons can be identical, every electron in an atom must have a different set of quantum numbers. The Pauli exclusion principle meant that only two electrons can exist in any one suborbital (spin up and spin down). In this way the orbitals are populated sequentially from lower to higher energy. When identical atoms combine to form a solid, their atomic orbitals overlap and the discrete energy levels of the isolated atom split into very closely spaced energies, effectively forming energy bands.

We turn now to Iron and the Fe 2p spectrum. Iron metal has 26 electrons, the majority of which are in filled orbitals. The only orbitals of relevance for chemical oxidation states are the 4 s and the 3d orbitals. The 4 s orbital is filled with two electrons and the 3d orbital, which can hold 10 electrons, is only partially filled with 6 electrons. The large number of unpaired electrons means that iron can potentially form high spin compounds in the presence of weak ligands (*e.g.* oxides, hydroxides halides and thiocyanates). In the creation of Fe^{2+}, iron loses two 4 s electrons and for Fe^{3+} it loses an additional 3d electron. Because the 4 s and 3d levels are close in energy, the filling of these orbitals can change depending on the local environment including external electromagnetic fields and ligand fields. When an X-ray ionises an electron (X-ray generated photoelectron) from the Fe 2p level, this immediately creates a hole leaving an unpaired electron in the 2p level and changes the potential that the escaping photoelectron experiences. Thus, upon ionisation the atomic potential changes transiently and the remaining electrons have to recouple in this transient potential [3,5]. This recoupling involves electrons both in the iron orbitals as well as those of surrounding ligands. In the case of oxides with an octahedral structure such as FeO and Fe_2O_3, the 3d levels, which are split into a 4-fold degenerate t_{2g} level and 2-fold degenerate e_g level, can be partially occupied due to partial covalent nature involving bonding with the O 2p levels. Moreover, the splitting between these states increases from ~ 1 eV to 2 eV in the presence of a core hole [5]. These rearrangements give rise to a large number of different final states called multiplets thereby spreading the intensity of the Fe 2p level over these different states. Under *no circumstances* can single peaks be used to represent either different types of oxides or Fe^{2+} or Fe^{3+} in these oxides. In summary, we here resonate with the words of Bagus et al. [5] "Clearly, in interpreting the XPS spectra, the angular momentum coupling and recoupling, the covalency, the ligand field splitting and the spin-orbit splitting, especially of core levels, must all be taken into account for a reliable description of the Fe 2p and Fe 3p XPS."

One other point which may address confusion among readers is that each iron atom only has one final state so all the multiplets are not generated in each atom; individual multiplet states occurs in separate atoms but because there are a range of transition states and because so many atoms are probed in a surface during XPS, the resultant spectrum collects information from all these states giving rise to the multiplet structure.

3. Dissecting prior literature

This work is based on the critical appraisal of the literature spanning the years since the publication of the seminal work by Biesinger et al. [8] on multiplet fitting of transition metals. Six separate years were chosen for the review including 2015, 2017, 2019, 2020, 2023 and 2024. Scopus was used as the search engine to find relevant papers based on the search terms "corrosion" AND "iron" AND "XPS". "Iron" was chosen over "steel" to simplify the review since in steels containing transition metal there can be significant overlap of Auger lines with the Fe 2p line. Nevertheless, some steel papers managed to get included. The fields that were searched included title, abstract and keywords. This search returned 1502 hits from the journals covered by Scopus from the period 2011–2024 (dated 9/11/2024). The number of papers for each year in

the review period are reported in Table 1. It should be noted that a number of papers were rejected on the basis that they were not related to corrosion of ferrous metals. It is likely that these were included through the assignment of Scopus generated keywords since none of these papers had the combination of keywords listed above in the search fields (title, abstract, keywords). The vast majority of the rejected papers were related to nano-sized Fe particles.

Fig. 2(a) and Table 1 shows the number of papers assessed in this study by year. This is not the total of all papers presenting XPS analysis of the Fe 2p spectral region in corrosion studies because Scopus only includes a limited number of journals (see journal selection criteria https://www.elsevier.com/en-au/products/scopus/content/content-policy-and-selection). However, these journals represent most, if not all of the eminent journals in the field. In total 220 papers were considered for the analyses presented below. Fig. 2(b) shows the percentage of papers using the chemistry fitting approach.

For the papers that were reviewed, the following criteria were used in their assessment:

General Information: (i) were the instrument manufacturer and operating conditions provided?

(ii) was a BE calibration provided such as C 1s peak position for adventitious carbon? Some authors reported spectrometer calibration which can't be used for BE calibration on charging samples and other used gold calibration. In the latter case it should be noted that the BE of evaporated gold depends on the gold particle size so a series of evaporation should be undertaken to ensure a large enough gold particle size to meet bulk gold characteristics [236,237].

Fe 2p: (iii) was *chemistry* or *envelope* fitting used? Here chemistry fitting refers to using single symmetric peaks to fit chemical species such as either Fe^{2+}, Fe^{3+}, FeO, Fe_3O_4, Fe_2O_3, FeOOH or any combination of these [2,6,8]. The examples of FeO and Fe_2O_3 are depicted in Fig. 1. Envelope fitting refers to fitting a pure reference compound then using the relative peak positions, ½ widths and intensities from the reference compound (fixed with respect to each other) to fit the unknown spectrum. This is the basis of the envelope method as described by Biesinger et al. [8]. It should be noted that the multiplet peak parameters are specific to a Shirley background. These values would need to be reoptimized for other backgrounds.

(iv) was a linear or non-linear background used?

(v) was placement of the background extrema positions sensible?

(vi) was the paper by Biesinger et al. [8] used as a reference?

(vii) was fitting performed on Fe 2p or $Fe2p_{3/2}$?

(viii) did the authors exhibit an understanding of the underlying spectroscopy or basic knowledge spin-orbit coupling?

A binary system was used to convert the answers to the questions above into statistics where "1" was yes and "0" was no. These were summed and expressed as a percentage of the total number of entries. One other observation that was considered was whether the paper was highly cited, *i.e.,* whether it was likely to be used as a reference for further propagating incorrect XPS data processing. However, no study was made of the direct impact of these papers on subsequent literature as has been done recently for S 2p [238].

Table 1
Number of papers found in SCOPUS, number of papers used in the review and the reference numbers for the papers themselves, by year.

Year	Number of papers in Scopus	Number of Papers in Review	Papers
2015	48	31	[10–40]
2017	48	23	[41–63]
2019	71	35	[64–98]
2020	88	48	[99–146]
2023	105	42	[147–188]
2024	120	45	[189–235]

4. Results

4.1. Instrument and BE calibration

This section addresses the general issues of proper protocol for reporting scientific data. We use the fundamental principles taught in high schools or first year science courses. This can be simply stated:

In describing experimental approaches and data treatment the author must include enough information to allow a reader to be able to reproduce the experiment and cross check the reported results.

This means that all instrument variables need to be reported including instrument types and operating conditions. It also means good reporting of sample attributes where available. In practice, it may be difficult to exactly reproduce a result due to small unknowns in experiments (e.g. a minor impurity in a chemical compound may have a major impact on the outcome of the experiment). Nevertheless, there is no good reason why authors should not include details about the instruments they used, how they were operated and how the reported data was processed. In the authors' opinions this should be explicitly written into the manuscript and not incorporated as a reference to earlier work. These days authors are often penalised for "self-plagiarism" by journals when they include experimental details word for word as written in one of their earlier publications. We suggest that plagiarism checks on experimental sections of papers be removed. It is far more important that journals hold to basic principles of scientific reporting than reject a paper because it has a relatively high percentage of the same text in the experimental section as a previously published paper. The reproduction of this text in multiple papers could even be seen as positive since it eliminates both awkward alternative descriptions of the experimental methods designed to avoid plagiarism and avoids referral to previous papers by the authors which leaves the current paper devoid of experimental details.

The data for reporting instrument details are summed up in Fig. 3(a). The data shows that there is a relatively high compliance with some level of reporting of the instrument details across all years examined. However, hidden within this statistic is the fact that the majority of papers did not report the operating conditions for the equipment or the method of data analysis. This means that researchers attempting to reproduce the experimental conditions cannot do so based on the information provided. This level of compliance is similar to that reported by Major et al. [239] who divided this category into full reporting and some reporting of instrument details.

There was poor reporting of the method used for BE referencing using the standard C 1 s BE value [240,241] (Fig. 3(b)). Moreover, the percentage of papers reporting C 1s seems to decline with time going from over 50 % in 2015 to around 30 % in 2024 (ANOVA p-value on gradient being 0.016). This represents a serious decline in standards (for this dataset) because all peak positions in XPS data need to have a BE calibration for the proper assignment of oxidation states. In the absence of this reference point it is not possible for a reader to quantitively assess the correctness of peak assignment within a paper and it becomes difficult to compare BE values between different papers. This omission contributes to the spread in reported BE values discussed below.

4.2. Identification of chemical species

The biggest issue noted in reviewing the literature is the use of the "chemistry approach" for the assignment of chemical species. An "at- a-glance" assessment of this problem can be made from inspection of Fig. 4. While the vast majority of papers have assignments for various chemical species in 707 eV to 713 eV region there are papers having incorrect assignments between 713 eV and 720 eV and a significant number have assignments above 720 eV. By way of explanation, the region between 713 eV and 720 eV is where the satellite structures from some of the oxides (or other compounds) becomes prominent and could be mistaken for a chemical species for those who are unaware of satellite

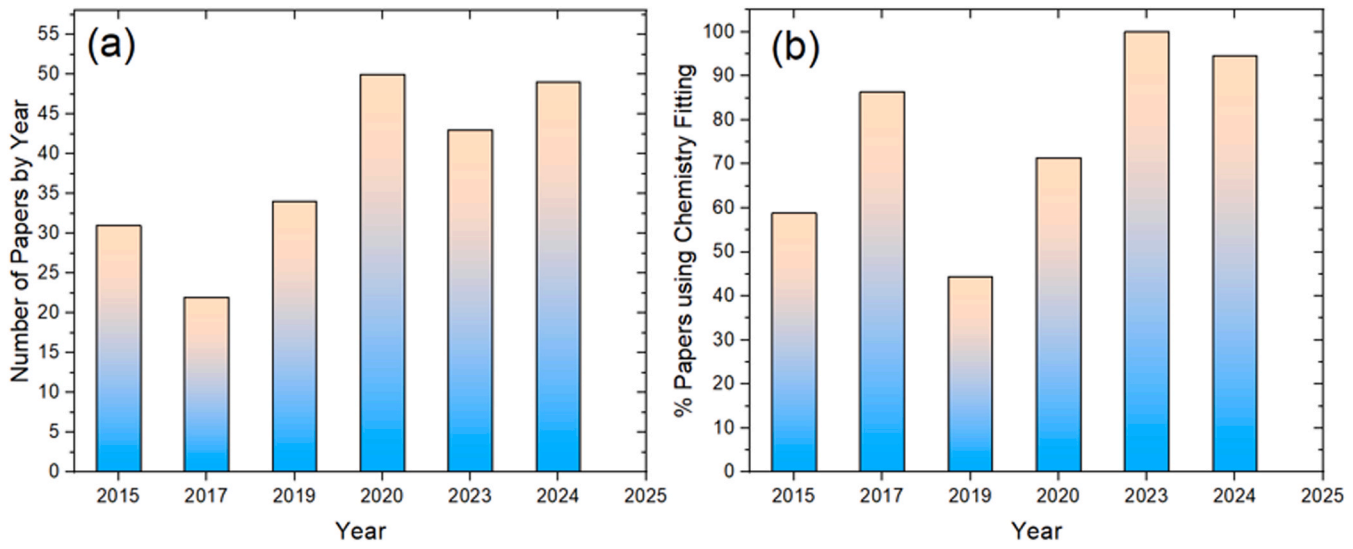

Fig. 2. (a) Actual number of papers included in this study by year and (b) percentage of papers using single symmetric peaks (chemistry fitting) to fit to either chemical species or oxidation states.

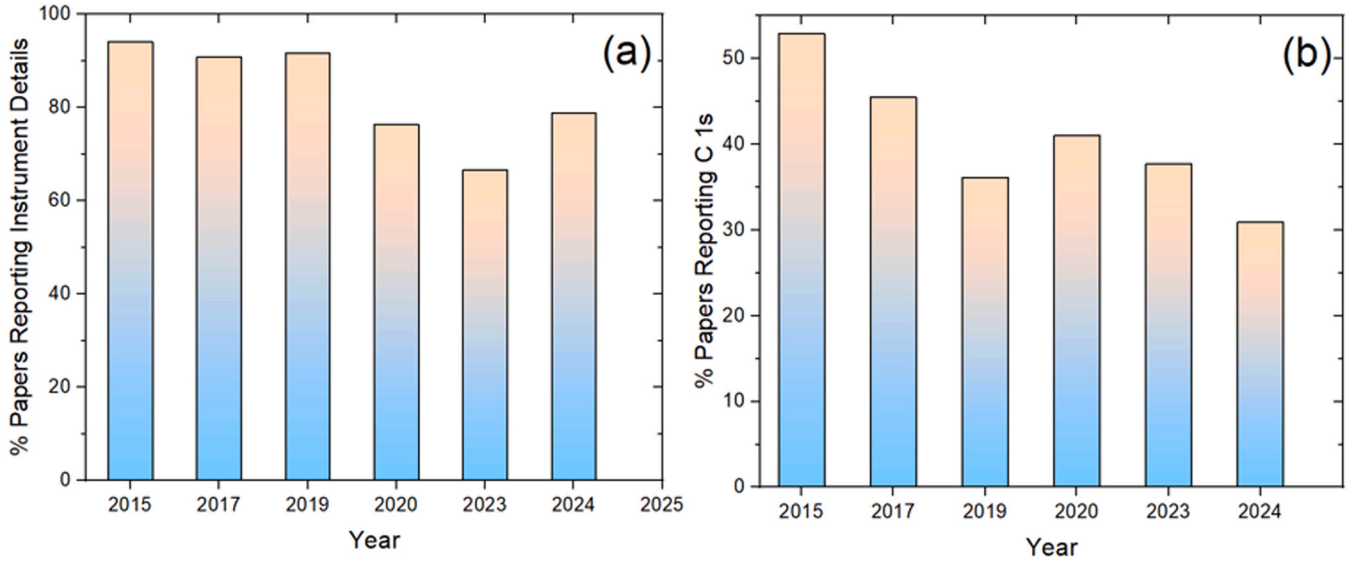

Fig. 3. Compliance, expressed as percentage, in reporting of (a) key instrumental and (b) C 1 s BE calibration data in experimental sections of papers reported by year. Here compliance indicates adherence to the standards of the scientific method, i.e. providing enough information for a researcher to reproduce the experimental results.

structures. The assignments above 720 eV clearly mis-identifies the Fe $2p_{1/2}$ peak for a new chemical species. This type of assignment represents a general ignorance of the quantum mechanics underlying orbital structure across the periodic table.

As noted in a previous study by the authors there is considerable confusion in the literature on austenitic steels about the assignment of oxide and hydroxide species in the Fe $2p_{3/2}$ spectrum. The origin of misassignment appears to be a mixture of:

(i) Absence of, or poor understanding of the physics behind photoelectron generation: there are studies where the authors do not seem to understand orbital angular momentum-electron spin coupling which leads to a spin-orbit splitting in the Fe 2p spectrum into Fe $2p_{3/2}$ and Fe$2p_{1/2}$ states; this is called branching. Branching ratios (relative intensities) and relative positions have fixed, well defined values. The BE separation of the $2p_{3/2}$ and $2p_{1/2}$ for the two oxides presented in Fig. 6(a) and (b) are indicated by the red arrows. In studies where this is not recognised, the Fe $2p_{1/2}$ is incorrectly assigned to a different oxidation state to those identified in the Fe $2p_{3/2}$ peak.

(ii) The majority of studies use chemistry fitting: single symmetric peaks to represent a chemical species or oxidation state. This approach bears no relation to the actual, underlying multiplet structure, meaning that the assignment of a peak position is quite arbitrary. There seems to be a trend where the assignment is designed to fit into the researcher's model of the surface rather than reflecting the actual oxide composition.

(iii) The use of NIST values: The NIST database (https://srdata.nist.gov/xps) contains a number of values for the peak maximum intensity for oxides but these were published prior to the field developing some understanding of multiplet structure of these peaks.

(iv) Incorrect spectrometer calibration leading to incorrect binding energy scale.

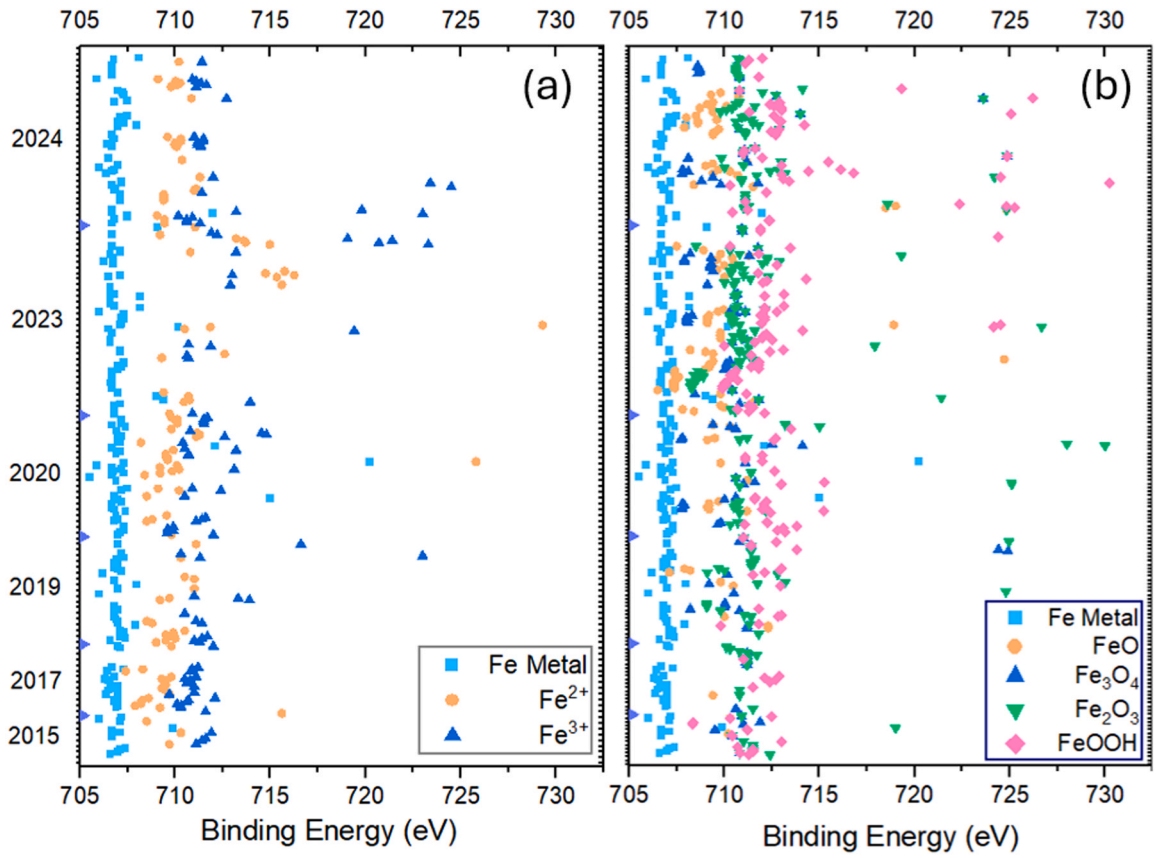

Fig. 4. Reported BE positions for the species nominated in the Figure legend; period covers 2015, 2017, 2019, 2020, 2023 and 2024. (a) Fe^{2+} and Fe^{3+} assignments and (b) Fe^0, FeO, Fe_3O_4, Fe_2O_3 and FeOOH. The assignment of data above 720 eV is ambiguous since the papers did not often recognise or understand the origins of spin-orbit splitting.

The issues mentioned above are shown in more detail in Fig. 5 where the Envelope (Fig. 5(a)) and Chemistry (Fig. 5(b)) fits are shown for a carbon steel exposed to 0.1 M NaCl with cerium and iodide ions present. XRD analysis of the surface identified Fe_2O_3, Fe_3O_4 and FeOOH. Using this information the multiplet envelopes of these components were fitted to the spectra. Here we also perform chemistry fitting using symmetric GL(30) peaks for the oxides and a metal component which has an asymmetric peak shape. GL(30) peak shapes are commonly used in the literature in this review. The three components labelled A, B and C were assigned to oxides based on common misconceptions about oxide positions in the literature. It can be seen from Fig. 5(c) that the percentage of each of these oxides is quite different for the Envelope vs the Chemistry fitting. This is despite both fits have similar RMS values indicating good optimisation. Given that the envelope approach better approximates the actual shape of the different components, it can be seen that the Chemistry fit is significantly in error. Fig. 5(d) highlights some of the other errors made in the literature including assigning new chemical species in regions where there are satellite structures and misinterpreting the Fe $2p_{1/2}$ peak for new chemical species; the $2p_{3/2}$ - $2p_{1/2}$ peaks are pairs for the same chemical species and represent the spin orbit splitting. We have explored the multiplet fitting of a mixture of Fe_2O_3 and FeOOH oxides in the presence of Fe_3O_4 and Fe metal in a little more detail in the supplementary material. As noted in our previous work fitting so many different species to one spectrum can be problematic[2]. In this case the presence of Fe_2O_3 and FeOOH covering the same energy range cannot be guaranteed to produce a unique result for these two species. However, the amount of Fe^{3+}, Fe_3O_4 and Fe metal may be good approximations to the actual composition whereas the actual amount of Fe_2O_3 and FeOOH cannot be replied upon.

Fig. 6 clearly reflects the problems listed above. Each of Fig. 6(a) for Fe_2O_3 and (b) for FeOOH have been divided into three binding energy regions as defined by cyan, green and yellow coloured rectangles representing "Chemistry Fitting", "Satellite Structures" and "Mistaken $2p_{1/2}$ for chemical species" respectively. Papers mistaking satellite structure as separate chemical state include [126,137,161,165,185,186,194,197,213,217,228,229,243] and those reporting the Fe $2p_{1/2}$ as a separate chemical state include [40,48,78,83,87,109,116,126,148,158,159,171,179,185,201,204,207,214,217,221,222,229,230,243,244]. In this third category papers making this assignment either did not quote a reference or referred to papers which did NOT make the assignment as insinuated by using the citation. Identifying the Fe $2p_{1/2}$ peak as a separate chemical state, makes up around 11 % of the total assignments in each oxide class in Fig. 6. This is clearly a concern because there is no scientific basis for the assignment but it seems to be now embedded in part of the scientific literature.

Examples of such problems are discussed in the following figures. We start with examples where the doublet $2p_{3/2}$ and $2p_{1/2}$ peaks have been confused with different oxidation states as presented in Fig. 7. In Fig. 7 (a) each species nominated on the $2p_{3/2}$ branch should have a corresponding peak at fixed intensity, position and relative half width in the $2p_{1/2}$ branch. In the example in Fig. 7(a) only FeOOH has intensity in both $2p_{3/2}$ and $2p_{1/2}$ components, but it is not clear that it is in the correct ratio or at the correct BE splitting. Fe_3O_4, for some unknown reason, is assigned to the Fe $2p_{1/2}$ peak. A proper search of the literature would establish this assignment is incorrect. Moreover, if there are 3 components in the Fe $2p_{3/2}$ region then there MUST be 3 corresponding components in the Fe $2p_{1/2}$. All other species have been incorrectly assigned including FeS, FeS_2, Fe_3O_4, $FePO_4$ and Fe_2O_3. In Fig. 7(b), none of the species have been correctly nominated since the branching is not recognised at all. In both examples the identification of chemical species

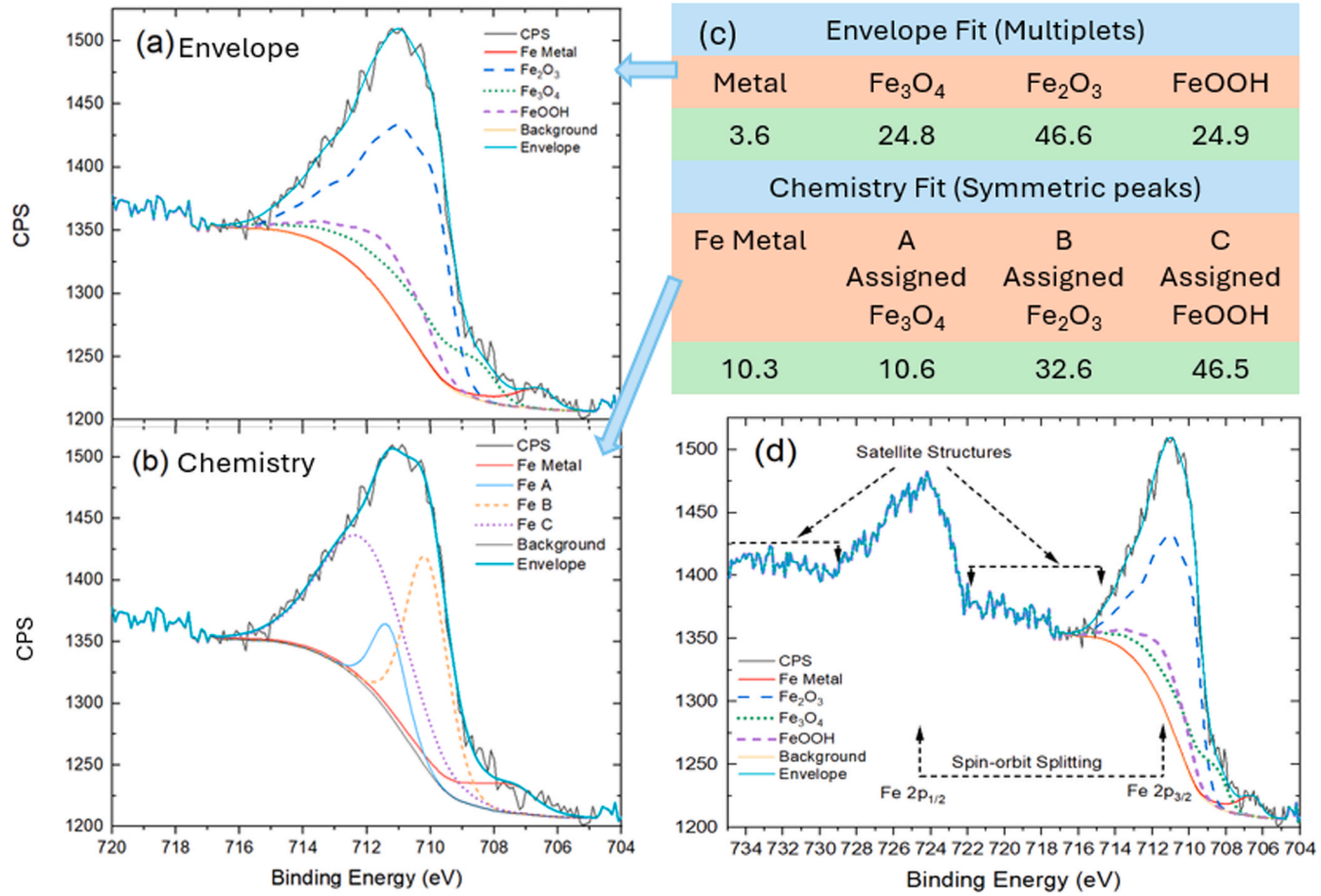

Fig. 5. Summary of Issues for XPS analysis of Fe $2p_{3/2}$ spectra for mild steel expose to 0.1 M NaCl from a study by El-Hashemy et al. [242]. (a) Envelope and (b) Chemistry fitting with (c) showing a summary of the analyses and (d) broader energy range for Fe 2p region showing spin-orbit splitting and location of satellite structures for iron oxides and hydroxides. GL(70) peaks were used for the multiplet components in (a) and GL(30) for the chemistry fitting for peaks "A", "B" and "C" in (b). For the metal a LA(1, 3.5,5) peak shape was used in both examples.

and any semiquantitative analyses will be useless in any attempt at characterising the material under examination.

Examples of chemical fitting are shown in Fig. 8 using figures from two papers [95,115]. Neither paper mentions the BE reference used to correct the BE scale, but the scale in Fig. 8(b) has been expanded by us to match the scale in Fig. 8(a). As noted in a previous study, reporting of fitting parameters is absent in many papers [245]. The peak assignment in the first example in Fig. 8(a) are as follows: 710.15 eV is Fe_3O_4, 711.5 eV is FeOOH and 712.8 eV is Fe_2O_3 [95]. In this instance Fe_3O_4 and FeOOH assignments appear to agree with the NIST value [6], however, 712.8 eV for Fe_2O_3 is nearly two electron volts higher than the corresponding NIST value for Fe_2O_3 and it is not clear where this value has come from. The authors quote three papers where they mention peaks assignments [246–248], but only one of the three has any XPS and it does not mention Fe_2O_3.

In Fig. 8(b), three peaks are used to fit the Fe $2p_{3/2}$ region. These peaks are labelled Fe, Fe_3O_4 and Fe_2O_3, at 707.96, 709.2 and 711.74 eV respectively. The first and most obvious thing to note is that there is no agreement with the positions of the Fe_3O_4 and Fe_2O_3 with different BEs given for the same species in Fig. 8(a) and (b). No BE reference is provided in the paper by Niu et al. [91] so it is not possible to check whether a correct reference has been used. The second observation to note is that, if a correct reference was used, then the peak at 707.96 eV is likely to be the lowest multiplet for FeO and Fe_3O_4 (they are not distinguishable [8]) which means that there is no Fe metal in this spectrum. In the case of Niu et al. [91] they have the assignments 707.96 eV for Fe, 711.74 eV for Fe_2O_3, 709.2 eV for Fe_3O_4. As with the previous paper it is not clear where these assignments originate. Only two citations are provided in the paragraph where these BEs are quoted. One reference does not explicitly mention any BEs and the other mentions the same BEs but without reference. It is these types of studies that lead to a state of confusion about BE assignment in oxides of iron in the literature. In this paper we advocate that the lowest multiplet peak positions be used as BE reference. In this case they are 708.4 eV for FeO, 708.4 eV for Fe_3O_4, 709.8 eV for Fe_2O_3 and 710.3 eV for FeOOH.

Another area of concern is the quality of fitting itself. Many studies over/underestimate the actual data envelope. Two examples include Fig. 7(b) and Fig. 8(b). In the former case the fit to the envelope is poor, particularly at the low BE end of the spectrum due in part to the Lorentzian-heavy line shapes employed, and therefore the square of residuals will not be statistically significant, meaning that the fit should be discarded (it should be discarded in any case because chemistry fitting is not appropriate). In the latter case, in addition to the problems mentioned for Fig. 8(b), the fit completely misses the satellite peak at around 720 eV. Peak intensities and half widths for components either side of this missed peak will be heavily influenced by this omission. There were a number of papers where the fit appeared not to be optimised at all.

4.3. *Chemistry vs envelope fitting*

One of the most important issues is what type of fitting models are used to extract information from the surface. There are two commonly used approaches to fitting Fe 2p data. The first is using single symmetric

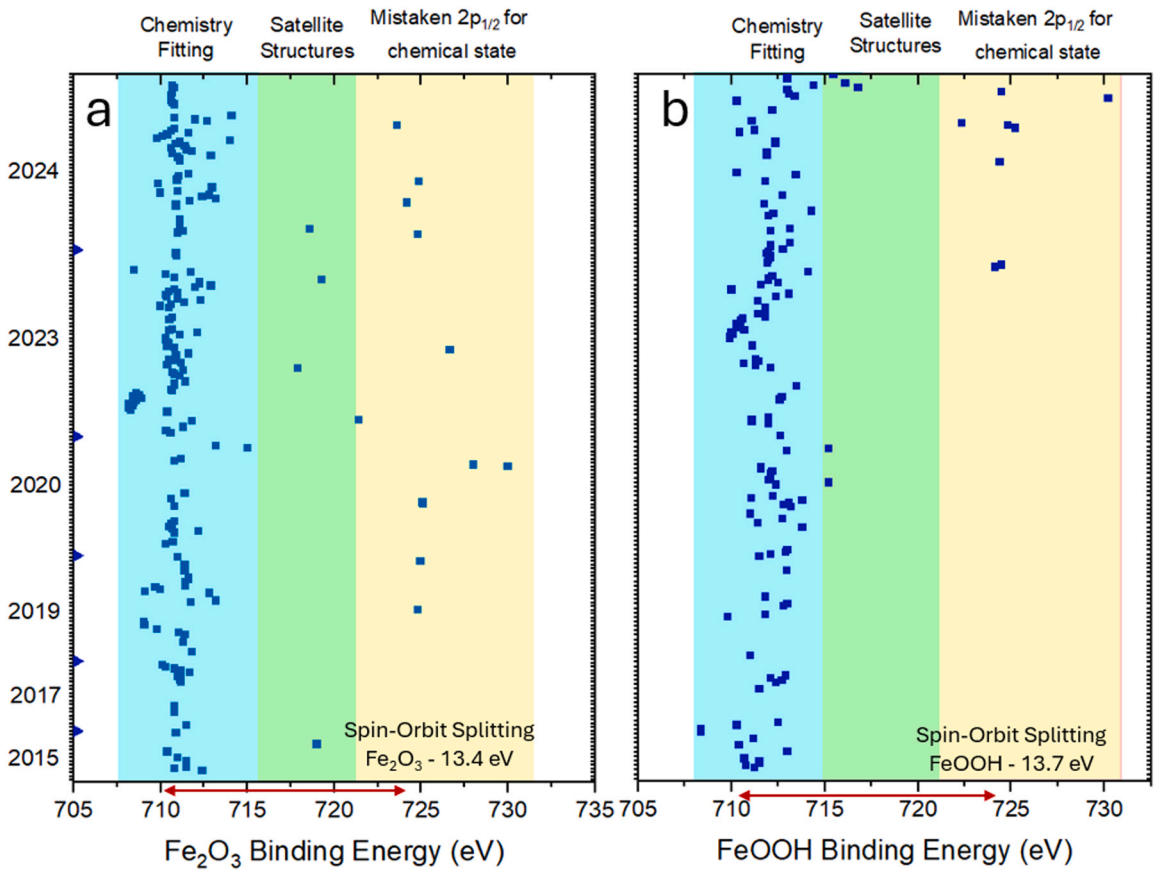

Fig. 6. Binding Energy (BE) assignments for (a) Fe_2O_3 and (b) FeOOH. Cyan, green and yellow rectangles indicate areas where binding energy assignment is based on chemistry fitting, misidentification of either satellite structure or assignment of the Fe $2p_{1/2}$ peak as a separate iron species. Note: these regions change from one oxide to another. Also indicated are the spin orbit splitting for Fe_2O_3 and FeOOH taken from our own data. Data span all years covered in the review.

peaks to represent different oxides (or other compounds) which is called Chemistry fitting. In the literature, this approach is applied to both the Fe 2p and Fe $2p_{3/2}$ region. The second approach is to fit the spectral envelope of reference compounds using pseudo-multiplets, fix the relative intensities and positions of the multiplets then apply them to the unknown spectrum. This is called envelope fitting. Hughes et al. [2] have already established, unequivocally, that chemistry fitting will not provide quantitative information on the surface composition for Fe $2p_{3/2}$ so a detailed analysis of the approach will not be discussed here. The following assessment, therefore, is only to examine how widespread the incorrect chemistry approach is applied rather than describe why it does not work.

Fig. 9 shows the extent to which each approach is used in the papers examined in this review. Clearly, at nearly 75 %, the chemistry approach is reported extensively in the literature. This means that any analysis that relies solely on the XPS data for determining the composition of the surface oxide or other species should be viewed as incorrect and it follows that the compositional analyses presented in these papers should also be considered incorrect. Moreover, if the conclusions reached in these studies rely on the XPS analysis then they should be considered as suspect.

As seen in Fig. 9, the vast majority of papers use the chemistry fit with only 4 % of papers use the envelope approach despite nearly 28 % of papers quoting the Biesinger et al. [8] paper with the number declining with time. Some of the papers that use the envelope approach to account for multiplets are the following references [79,130,242,249]. It should be noted that even the envelope approach can fail to converge to a meaningful solution when there are too many species included in the fit [2]. This is particularly a problem when FeO and Fe_3O_4 are present on the surface in addition to metal because (i) they both have multiplet components around 708.4 eV, (ii) spectral intensity from the asymmetric metal peak shape contributes to the region above 708.0 eV as does (iii) an increase in the background from the metal peak due to the oxide overlayer [2]. In this instance it is best practice not to fit the spectra at all rather than present incorrectly fitted spectra.

From Fig. 9, it can be seen that the envelope and chemistry categories combined add to around 77 %, leaving 23 % outside these two categories. These residual papers represent a 3rd significant class of papers that the authors of this article had not expected to be this prevalent. The authors of this 3rd class of papers have chosen to present only the spectra rather than pursue a curvefitting approach. The choice not to perform curvefitting in these papers was often based on a recognition that fitting was complex and perhaps impossible to do correctly with the chemical species that they were examining.

Fig. 9 also shows the percentage of papers which attempt to fit the full Fe 2p range rather than just the Fe $2p_{3/2}$ region of the Fe 2p spectrum. Fitting the full Fe 2p spectrum may seem to be a good approach, but it is potentially fraught with more problems than fitting the Fe $2p_{3/2}$ part of the Fe2p spectrum. The first and major problem is where to set the limits for background calculation and what type of background to use. Current recommendations suggest that a Tougaard background be used and that the higher BE position for the background be set well above the Fe $2p_{1/2}$ peak position [250,251]. The second problem is that there are significant loss lines from both the Fe $2p_{3/2}$ and Fe $2p_{1/2}$ peaks which are well separated from these major features in the Fe 2p spectra [252]. In the case of the Fe $2p_{3/2}$ peak, these loss lines fall beneath the Fe $2p_{1/2}$ peak and at even higher BEs for the Fe $2p_{1/2}$ so the background has to be chosen to be at a higher BE than the last of these loss lines. On the background itself, only 55 % of the papers used the Shirley background with the rest using linear or not fitting the Fe 2p region at all.

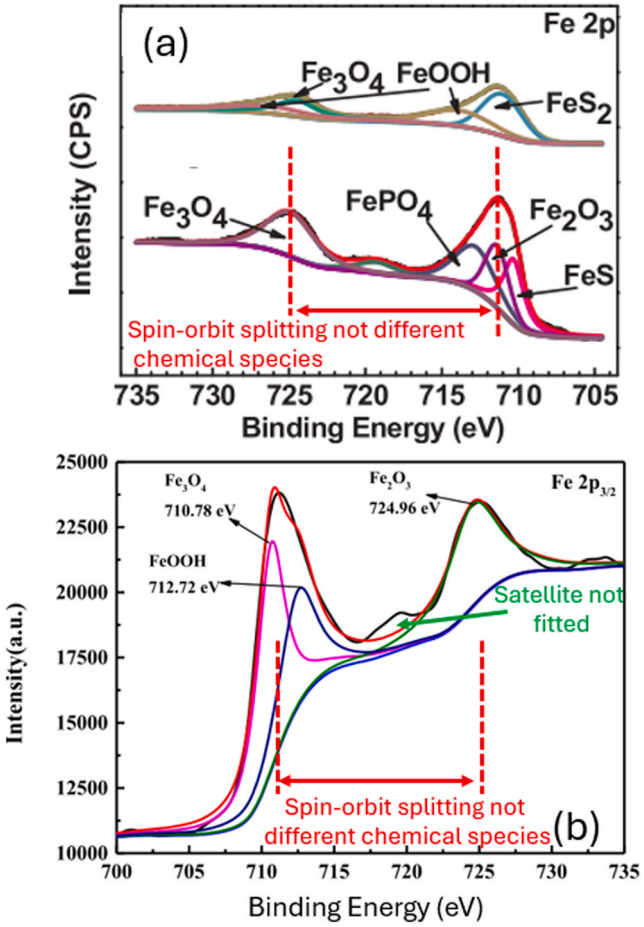

Fig. 7. Examples of chemical states being assigned to peaks generated through spin-orbit splitting (a) only FeOOH has intensity in both $2p_{3/2}$ and $2p_{1/2}$ components [78] (Reproduced with permission licence No.: 5995100169812) and (b) incorrect assignment of oxides [83] (Reproduced with permission licence No.: 1626533–1). Both figures indicate the spin-orbit splitting and (b) indicates a satellite peak that is not fitted.

Research into how to deal with the background is an active area with new approaches occasionally emerging. There is another approach for treating the Fe 2p region based on a process using the semiclassical dielectric response function which yields the composite spectrum but with symmetric peaks [250]. In this approach the inelastic background and satellite peaks are removed but the multiplet structure remains and needs to be dealt with. Tougaard's group has put a lot of effort into addressing background removal [251].

5. Discussion

In this paper we have identified that there are three areas in which the treatment of the Fe 2p XPS region falls down:

1. Misidentification of the Fe $2p_{1/2}$ peak as a separate chemical state,
2. Misidentification of Fe $2p_{3/2}$ satellite structure as a separate chemical state
3. Use of Chemistry fitting to establish the presence of different Fe-oxides or other compounds and determine their relative composition.

The issues related to points 1 and 2 above have been discussed in detail in the body of the paper. They relate to ignorance of the physical processes behind the spectroscopy of the Fe 2p region. Issue 1 is more fundamental than issue 2 and possibly lies in the backgrounds and qualifications of those using XPS with some researchers perhaps not coming into contact with quantum mechanics of the atom during their undergraduate education or careers. Satellite structure is a more complex topic and really relies on familiarity with

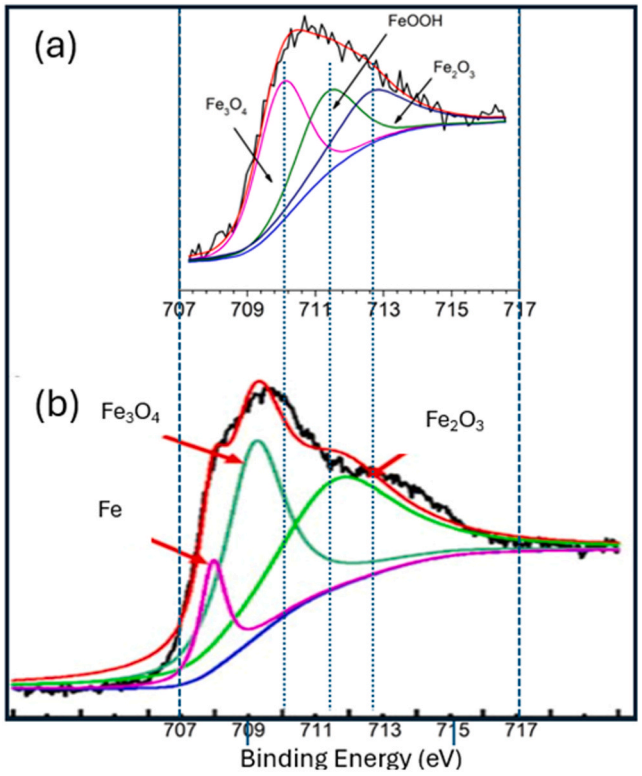

Fig. 8. Two examples of chemical fitting of Fe $2p_{3/2}$ peak using a number of symmetric components. (a) is from Chen et al. [95] (Copyright © 2019 Chen, Deng, Liu and Zhang) and (b) is from Niu et al. [91] (Reproduced with permission licence No.: 1626537–1). Fine dotted lines extend from the peak maxima in (a) to the figure in (b) to indicate where the peaks in a fall in (b). Note that there is no real agreement between the assignments.

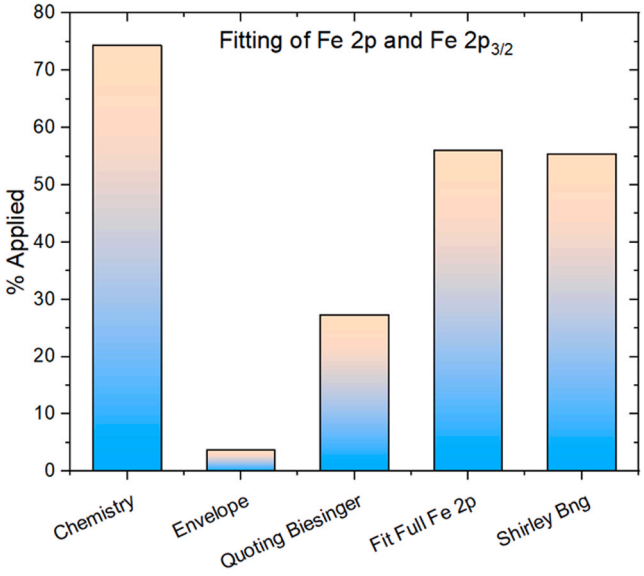

Fig. 9. Percentage compliance for using the Chemistry and Envelope fitting approach, percentage papers quoting the Biesinger paper [8], percentage fitting of the full Fe 2p region and percentage using the Shirley background. Note: The chemical approach has been proven to provide no useful information about the oxide composition on the surface [2]. Data Span 2015 to 2024.

empirical studies in the literature examining satellite structure of specific compounds or familiarity with theoretical QM studies of these structures. In both instances, however, information is available on-line as well as in the literature and reference sources (e.g. undergraduate books on quantum mechanics).

The issue of multiplet structure and the need to use a fitting approach to accommodate this feature is another complex problem. First, the physics is more complex than that of satellite structures, so researchers need to be guided by the experts in this area rather than make up their own rules. Second, it should be recognised that envelope fitting is a midstep between full fitting, based on theory, and chemistry fitting. Fig. 1 clearly demonstrates that the chemistry approach falls short in it's very poor reproduction of the XPS envelopes of oxides. The aim of the envelope approach is to reproduce the XPS peak shape using a number of peaks based loosely on the underlying multiplet structure. It is limited to determining the percentage of different oxide (or other chemicals) contribution to the Fe $2p_{3/2}$ peak. Intensities derived from this approach should not be used directly in quantitative analysis to determine atomic ratios with respect to other species. Instead, the full Fe 2p intensity, determined from either survey or high resolution scans, should be used then the fraction of a particular oxide can be determined using the percentages derived from envelope fitting results on the Fe $2p_{3/2}$ peak.

As to actions that need to be undertaken, there is an immediate need for a vast improvement in the way XPS data for the Fe 2p region is reported and analysed. The following recommendations for specific parties are suggested:

a. *Authors*: Generally better reporting of instrument type and operation is required to bring it to an appropriate standard for scientific reporting. With respect to fitting, the envelope approach, rather than the chemistry approach should be adopted. If this is not possible then only the experimental data should be reported.
b. *Journals*: Adopt new standards to ensure that reporting is up to basic scientific standards. A general practice to be implemented is to have a combined basic scientific reporting as well as a plagiarism check during the manuscript submission stage for authors. In case of flaws, they can and should be repaired prior to final submission and further editorial and reviewer handling. This could be done through basic questionnaires to the authors and implementation of large language models as part of an AI-assisted manuscript submission process.
c. *Journals*: Develop methods to screen for limited or flawed data analysis procedures. Since it is possible to automate plagiarism tests, then why not look for indicators of the data analysis approach, thereby essentially relieving responsibility from editors and reviewers to identify these fundamental errors. This will have the added benefit of saving time for reviewers having to address obvious sub-standard analysis. At some stage in the future perhaps AI-assisted manuscript review could occur at the time of submission.
d. *Journals:* Remove impediments to authors to fully report experimental procedures such targeted plagiarism tests on experimental sections of papers.
e. *Other approaches* – scientific committees within institutions to examine papers prior to sending to review which will develop a reputation of high standards for journals that adopt this approach.

6. Conclusions

In this paper the authors have reviewed the fitting of XPS spectra of the Fe 2p region in a large number of papers from the corrosion literature. These papers have been identified using a SCOPUS search and represent papers published in the most reputable journals in the field. A number of shortcomings have been found in the literature. These include:

1. Poor reporting of details of experimental techniques.
2. Poor understanding of the physics of the spectroscopy of the Fe 2p region. This has led to incorrect analysis of the Fe 2p region due to the adoption of poor fitting approaches.
3. Poor use of references with authors referring to papers quoting Fe 2p BEs in the text but where the reference does not itself make the quoted assignment.
4. In a few cases leading to complete fabrication of peak assignments.

The authors offer guidance to the research community on proper scientific reporting and data analysis approaches as well as some suggestions for the improvement of the status quo in the literature providing guidance for both authors and journals. These suggestions include recommendations and guidance (i) to authors to elevate the level of detail and completeness of scientific reporting and data analysis prior to manuscript submission, and (ii) to journals to enhance their AI-assisted plagiarism and data analysis assessment prior to and upon manuscript submission to relieve the responsibility imposed on journal editors and reviewers during the subsequent manuscript handling stages.

CRediT authorship contribution statement

Nick C. Wilson: Writing – review & editing, Writing – original draft, Validation, Formal analysis, Data curation. **Mol Arjan:** Writing – review & editing, Writing – original draft, Visualization, Supervision, Project administration, Formal analysis, Data curation, Conceptualization. **Prasaanth Ravi Anusuyadevi:** Writing – review & editing, Writing – original draft, Visualization, Validation, Investigation, Formal analysis, Data curation. **Thomas J. Raeber:** Writing – review & editing, Writing – original draft, Validation, Formal analysis, Data curation. **Anthony E. Hughes:** Writing – review & editing, Writing – original draft, Visualization, Validation, Methodology, Investigation, Formal analysis, Data curation, Conceptualization. **Christopher D. Easton:** Writing – review & editing, Writing – original draft, Validation, Formal analysis, Data curation.

Declaration of Competing Interest

The authors declare that they have no known competing financial interests or personal relationships that could have appeared to influence the work reported in this paper.

Appendix A. Supporting information

Supplementary data associated with this article can be found in the online version at doi:10.1016/j.corsci.2025.113357.

Data availability

Data will be made available on request.

References

[1] J.E. Castle, Module to guide the expert use of X-ray photoelectron spectroscopy by corrosion scientists, J. Vac. Sci. Technol. A 25 (1) (2006) 1–27.
[2] A.E. Hughes, et al., Interpretation of complex x-ray photoelectron peak shapes. I. case study of fe 2p3/2 spectra, J. Vac. Sci. Technol. A Vac. Surf. Films 42 (5) (2024).
[3] P.S. Bagus, et al., Multiplet splitting for the XPS of heavy elements: dependence on oxidation state, Surf. Sci. 643 (2016) 142–149.
[4] M.A. Isaacs, A. Graf, D.J. Morgan, XPS insight note: multiplet splitting in X-Ray photoelectron spectra, Surf. Interface Anal. 57 (4) (2025) 285–290.
[5] P.S. Bagus, et al., Combined multiplet theory and experiment for the fe 2p and 3p XPS of FeO and Fe2O3, J. Chem. Phys. 154 (9) (2021).
[6] A.E. Hughes, et al., Interpretation of complex x-ray photoelectron peak shapes. Ii. case study of fe 2p3/2 fitting applied to austenitic stainless steels 316 and 304, J. Vac. Sci. Technol. A Vac. Surf. Films 42 (5) (2024).

[7] M.R. Linford, et al., Proliferation of faulty materials data analysis in the literature, Microsc. Microanal. 26 (1) (2020) 1–2.
[8] M.C. Biesinger, et al., Resolving surface chemical states in XPS analysis of first row transition metals, oxides and hydroxides: cr, mn, fe, co and ni, Appl. Surf. Sci. 257 (7) (2011) 2717–2730.
[9] R. Eisberg, R. Resnick, Quantum Physics of Atoms, Molecules, Solids, Nucleii and Particles, Chapter 10,. first ed., John Wiley & Sons, New York, 1974.
[10] Y.G. Ko, et al., Characterizations of electrodeposited uranium layer on stainless steel disc, Colloids Surf. A Physicochem. Eng. Asp. 487 (2015) 121–130.
[11] N. El Hamdani, et al., Alkaloids extract of retama monosperma (L.) boiss. Seeds used as novel eco-friendly inhibitor for carbon steel corrosion in 1M HCl solution: electrochemical and surface studies, Appl. Surf. Sci. 357 (2015) 1294–1305.
[12] G.D. Eyu, et al., Effect of hydrodynamics and surface roughness on the electrochemical behaviour of carbon steel in CSG produced water, Appl. Surf. Sci. 357 (2015) 506–515.
[13] H. Nan, et al., Protection of NdFeB magnets by corrosion resistance phytic acid conversion film, Appl. Surf. Sci. 355 (2015) 1215–1221.
[14] H. Li, et al., Effect of tin on the corrosion behavior of sea-water corrosion-resisting steel, Mater. Des. 84 (2015) 1–9.
[15] W. Liu, et al., Corrosion performance of 3%Cr steel in CO2-H2S environment compared with carbon steel, Mater. Corros. 66 (11) (2015) 1232–1244.
[16] F. Cao, et al., The corrosion inhibition effect of phytic acid on 20SiMn steel in simulated carbonated concrete pore solution, Corros. Sci. 100 (2015) 365–376.
[17] D. Zhang, K. Huang, Fe–Ni–Cr alloy as bipolar plate of PEMFC by multi-steps surface modification, Int. J. Hydrog. Energy 40 (39) (2015) 13538–13548.
[18] R. Steinberger, et al., XPS study of the effects of long-term Ar+ ion and ar cluster sputtering on the chemical degradation of hydrozincite and iron oxide, Corros. Sci. 99 (2015) 66–75.
[19] K. Boumhara, et al., Artemisia mesatlantica essential oil as Green inhibitor for carbon steel corrosion in 1M HCl solution: electrochemical and XPS investigations, J. Ind. Eng. Chem. 29 (2015) 146–155.
[20] Y. Zhang, et al., Structural evolution of nanoscale Zero-Valent iron (nZVI) in anoxic Co2+ solution: interactional performance and mechanism, Sci. Rep. 5 (1) (2015) 13966.
[21] M. Mihelčič, et al., Novel sol–gel based selective coatings: from coil absorber coating to high power coating, Sol. Energy Mater. Sol. Cells 140 (2015) 232–248.
[22] Y. Liu, et al., Influence of biocompatible metal ions (Ag, Fe, Y) on the surface chemistry, corrosion behavior and cytocompatibility of Mg–1Ca alloy treated with MEVVA, Colloids Surf. B Biointerfaces 133 (2015) 99–107.
[23] D. Sarada Kalyani, et al., Electrochemical and surface analytical studies of carbon steel protected from corrosion in a low-chloride environment containing a phosphonate-based inhibitor, Res. Chem. Intermed. 41 (8) (2015) 5007–5032.
[24] Y.-f Xu, et al., Corrosion behavior of Ti–Nb–Ta–Zr–Fe alloy for biomedical applications in ringer's solution, Trans. Nonferrous Met. Soc. China 25 (8) (2015) 2556–2563.
[25] J. Rechmann, et al., Surface functionalization of oxide-covered zinc and iron with phosphonated phenylethynyl phenothiazine, Langmuir 31 (26) (2015) 7306–7316.
[26] R.-C. Zeng, et al., In vitro corrosion of as-extruded Mg–Ca alloys—the influence of Ca concentration, Corros. Sci. 96 (2015) 23–31.
[27] R.D. Slaton, et al., The transformation of α-Fe nanoparticles into multi-domain FeNi–M3O4 (M = Fe, Ni) heterostructures by galvanic exchange, J. Mater. Chem. C. 3 (24) (2015) 6367–6375.
[28] S. Ningshen, M. Sakairi, Corrosion degradation of AISI type 304L stainless steel for application in nuclear reprocessing plant, J. Solid State Electrochem. 19 (12) (2015) 3533–3542.
[29] D.J. Park, et al., A study of the oxidation of FeCrAl alloy in pressurized water and high-temperature steam environment, Corros. Sci. 94 (2015) 459–465.
[30] S.-A. Park, et al., Effect of chloride ions on the corrosion behavior of low-alloy steel containing copper and antimony in sulfuric acid solution, Met. Mater. Int. 21 (3) (2015) 470–478.
[31] L. Marchetti, et al., XPS study of Ni-base alloys oxide films formed in primary conditions of pressurized water reactor, Surf. Interface Anal. 47 (5) (2015) 632–642.
[32] N. Ochoa, et al., CO2 corrosion resistance of carbon steel in relation with microstructure changes, Mater. Chem. Phys. 156 (2015) 198–205.
[33] D. Rodriguez, D. Chidambaram, Oxidation of stainless steel 316 and nitronic 50 in supercritical and ultrasupercritical water, Appl. Surf. Sci. 347 (2015) 10–16.
[34] H. Gao, et al., Controllable fabrication of stable superhydrophobic surfaces on iron substrates, RSC Adv. 5 (51) (2015) 40657–40667.
[35] A. Liu, J. Liu, W.-x Zhang, Transformation and composition evolution of nanoscale zero valent iron (nZVI) synthesized by borohydride reduction in static water, Chemosphere 119 (2015) 1068–1074.
[36] X. Liu, et al., Using high-temperature mechanochemistry treatment to modify iron oxide and improve the corrosion performance of epoxy coating – I. High-temperature ball milling treatment, Corros. Sci. 90 (2015) 451–462.
[37] I. Samusawa, K. Shiotani, Influence and role of ethanol minor constituents of fuel grade ethanol on corrosion behavior of carbon steel, Corros. Sci. 90 (2015) 266–275.
[38] X. Jiang, et al., Enhanced paramagnetic Cu2+ ions removal by coupling a weak magnetic field with zero valent iron, J. Hazard. Mater. 283 (2015) 880–887.
[39] C. Zhao, et al., Spontaneous formation of mono-n-butyl phosphate and mono-n-hexyl phosphate thin films on the iron surface in aqueous solution and their corrosion protection property, RSC Adv. 5 (67) (2015) 54420–54432.
[40] L. Wei, et al., Formation mechanism and protective property of corrosion product scale on X70 steel under supercritical CO2 environment, Corros. Sci. 100 (2015) 404–420.
[41] X. Li, et al., Electrochemical micromachining with fiber laser masking for 304 stainless steel, IOP Conf. Ser. Mater. Sci. Eng. 250 (1) (2017) 012056.
[42] J.C. Orozco, et al., Effects of oxidation-nitridation in the presence of water vapor on ASTM A335 P92 steel using SEM-EDS and XPS characterization techniques, J. Phys. Conf. Ser. 935 (1) (2017) 012056.
[43] Y. Wu, et al., Tribological and anticorrosion behaviour of novel xanthate-containing triazine derivatives in water-glycol, Tribology Int. 110 (2017) 113–124.
[44] Y. Cheng, et al., Fabrication of Cu–CuO–Fe2O3/Fe anti-sticky and superhydrophobic surfaces on an iron substrate with mechanical abrasion resistance and corrosion resistance, New J. Chem. 41 (12) (2017) 5205–5214.
[45] F.D. Franco, et al., Effect of high temperature oxidation process on corrosion resistance of bright annealed ferritic stainless steel, J. Electrochem. Soc. 164 (13) (2017) C869.
[46] H. Shi, et al., Corrosion behavior of High-Nitrogen stainless steel in NaCl solution, Int. J. Electrochem. Sci. 12 (12) (2017) 11298–11308.
[47] Z. Sanaei, T. Shahrabi, B. Ramezanzadeh, Synthesis and characterization of an effective Green corrosion inhibitive hybrid pigment based on zinc acetate-Cichorium intybus l leaves extract (ZnA-CIL.L): electrochemical investigations on the synergistic corrosion inhibition of mild steel in aqueous chloride solutions, Dyes Pigments 139 (2017) 218–232.
[48] Y. Zhou, Y. Zuo, B. Lin, The compounded inhibition of sodium molybdate and benzotriazole on pitting corrosion of Q235 steel in NaCl + NaHCO3 solution, Mater. Chem. Phys. 192 (2017) 86–93.
[49] Y. Hao, et al., Phytic acid doped polyaniline containing epoxy coatings for corrosion protection of Q235 carbon steel, Appl. Surf. Sci. 419 (2017) 826–837.
[50] D. Rodriguez, et al., Surface chemistry and corrosion behavior of inconel 625 and 718 in subcritical, supercritical, and ultrasupercritical water, Appl. Surf. Sci. 404 (2017) 443–451.
[51] H. Ma, et al., Study on deposits containing rich fluorine, boron, and ammonium on the heating surface of a flue gas cooler in a 300 MW Coal-Fired boiler, Energy Fuels 31 (5) (2017) 4742–4747.
[52] D. Blanco, et al., Antifriction and antiwear properties of an ionic liquid with Fluorine-Containing anion used as lubricant additive, Tribology Lett. 65 (2) (2017) 66.
[53] S.P. Chenakin, et al., Ultrasonic impact treatment of CoCrMo alloy: surface composition and properties, Appl. Surf. Sci. 408 (2017) 11–20.
[54] J. Wang, et al., Effect of rolling method and sensitization treatment on the microstructure and passive properties in 2101 duplex stainless steel, Int. J. Electrochem. Sci. 12 (7) (2017) 6492–6505.
[55] M. Corrales-Luna, et al., Influence of the immersion time and temperature on the corrosion of API X52 steel in an aqueous salt medium, Int. J. Electrochem. Sci. 12 (7) (2017) 6729–6741.
[56] M.R. Ardigo-Besnard, et al., Effect of surface finishing on the oxidation behaviour of a ferritic stainless steel, Appl. Surf. Sci. 412 (2017) 196–206.
[57] X.-H. Sun, et al., Electrochemical and microscopic investigation on passive behavior of ductile iron in simulated cement-mortar pore solution, Constr. Build. Mater. 150 (2017) 703–713.
[58] M. Dadfar, et al., Surface and corrosion properties of modified passive layer on 304 stainless steel as bipolar plates for PEMFCs, Int. J. Hydrog. Energy 42 (41) (2017) 25869–25876.
[59] L. Jinlong, et al., Comparison of corrosion resistance of electrodeposited pure ni and nanocrystalline Ni–Fe alloy in borate buffer solution, Mater. Chem. Phys. 202 (2017) 15–21.
[60] C.-j Wang, Q.-j Chen, H.-x Xia, Optimization of Cr/Mo molar ratio in FeCoCrMoCBY alloys for high corrosion resistance, Trans. Nonferrous Met. Soc. China 27 (12) (2017) 2663–2672.
[61] D. Kosugi, et al., Effect of the addition of molybdenum on the structure and corrosion resistance of Zinc–Iron plating, Coatings 7 (2017), https://doi.org/10.3390/coatings7120235.
[62] X. Dai, et al., Characterizing and exploring the mechanism of formation of corrosion scales by reusing advanced-softened, silica-rich, oilfield-produced water (ASOW) in a steam-injection boiler, J. Chem. Technol. Biotechnol. 92 (2) (2017) 382–390.
[63] D. Zhou, et al., Corrosion behavior of tinplate in aerated and deaerated NaCl solution, Int. J. Electrochem. Sci. 12 (1) (2017) 639–651.
[64] T. Duan, et al., Long-term field exposure corrosion behavior investigation of 316L stainless steel in the deep sea environment, Ocean Eng. 189 (2019) 106405.
[65] S. Chimenti, et al., In-situ phosphatization and enhanced corrosion properties of films made of phosphate functionalized nanoparticles, React. Funct. Polym. 143 (2019) 104334.
[66] X. Li, et al., Microstructure of passive film on steel in synthetic concrete pore solution in presence chloride and nitrite, Int. J. Electrochem. Sci. 14 (9) (2019) 8624–8638.
[67] Y. Tian, M. Zheng, Inhibition effect of silicate and molybdate on the corrosion of SS 316 in neutral corrosive solution at high temperature, Mater. Res. Express 6 (9) (2019).
[68] J. Sui, et al., Initial oxidation mechanisms of stainless steel sanicro 28 (35Fe27Cr31Ni) exposed to KCl, NaCl, and K2CO3 under dry and humid conditions at 535 °C, Corros. Sci. 155 (2019) 29–45.
[69] F. Arjmand, J. Wang, L. Zhang, Zinc addition and its effect on the corrosion behavior of a 30% cold forged alloy 690 in simulated primary coolant of pressurized water reactors, J. Alloy. Compd. 791 (2019) 1176–1192.

[70] J. Ren, et al., Corrosion behavior of an al added high-Cr ODS steel in supercritical water at 600 °C, Appl. Surf. Sci. 480 (2019) 969–978.
[71] M. Kovendhan, et al., Study of stainless steel electrodes after electrochemical analysis in sea water condition, Environ. Res. 173 (2019) 549–555.
[72] C. Merola, et al., Nanometer resolved real time visualization of acidification and material breakdown in confinement, Adv. Mater. Interfaces 6 (10) (2019) 1802069.
[73] Y. Qiu, et al., Microstructural evolution, electrochemical and corrosion properties of AlxCoCrFeNiTiy high entropy alloys, Mater. Des. 170 (2019) 107698.
[74] B. Guitián, X.R. Nóvoa, A. Pintos, Development of conversion coatings on iron via corrosion in LiPF6 solution, Electrochim. Acta 304 (2019) 428–436.
[75] X. Liu, et al., Environmentally friendly Zr-based conversion nanocoatings for corrosion inhibition of metal surfaces evaluated by multimodal X-ray analysis, ACS Appl. Nano Mater. 2 (4) (2019) 1920–1929.
[76] M. Ramezanzadeh, et al., Mild steel surface eco-friendly treatment by Neodymium-based nanofilm for fusion bonded epoxy coating anti-corrosion/adhesion properties enhancement in simulated seawater, J. Ind. Eng. Chem. 72 (2019) 474–490.
[77] W. Phillips, D. Chidambaram, Corrosion of stainless steel 316L in molten LiCl-Li2O-Li, J. Nucl. Mater. 517 (2019) 241–253.
[78] J. Wang, et al., The performance and mechanism of bifunctional biocide sodium pyrithione against sulfate reducing bacteria in X80 carbon steel corrosion, Corros. Sci. 150 (2019) 296–308.
[79] A.S. Al-Badran, A. Mechler, Corrosion inhibition of iron surfaces with phosphatidic acid, Eur. J. 3 (3) (2019) 128–134.
[80] Q. Yu, et al., Novel N, P-containing oil-soluble ionic liquids with excellent tribological and anti-corrosion performance, Tribology Int. 132 (2019) 118–129.
[81] A.G. Talkhan, et al., Corrosion study of carbon steel in CO2 loaded solution of N-methyldiethanolamine and l-arginine mixtures, J. Electroanal. Chem. 837 (2019) 10–21.
[82] M.M. Khan, I. Shabib, W. Haider, A combinatorially developed Zr-Ti-Fe-Al metallic glass with outstanding corrosion resistance for implantable medical devices, Scr. Mater. 162 (2019) 223–229.
[83] Y. Gui-Rong, et al., Corrosion behavior of 20# steel at initial stage under the (CO2/aqueous solution) gas-liquid two-phase plug flow condition, Mater. Res. Express 6 (2019) 6.
[84] F. Ning, X. Wu, J. Tan, Crevice corrosion behavior of alloy 690 in high-temperature water, J. Nucl. Mater. 515 (2019) 326–337.
[85] M. Tabatabaei majd, et al., Development of a high-performance corrosion protective functional nano-film based on poly acrylic acid-neodymium nitrate on mild steel surface, J. Taiwan Inst. Chem. Eng. 96 (2019) 610–626.
[86] X. Li, et al., Effect of extremely aggressive environment on the nature of corrosion scales of HP-13Cr stainless steel, Appl. Surf. Sci. 469 (2019) 146–161.
[87] B. Dong, et al., Corrosion mechanism and applicability assessment of N80 and 9Cr steels in CO2 auxiliary steam drive, J. Mater. Eng. Perform. 28 (2) (2019) 1030–1039.
[88] G. Bahlakeh, B. Ramezanzadeh, M. Ramezanzadeh, The role of chrome and zinc free-based neodymium oxide nanofilm on adhesion and corrosion protection properties of polyester/melamine coating on mild steel: experimental and molecular dynamics simulation study, J. Clean. Prod. 210 (2019) 872–886.
[89] K.F. Quiambao, et al., Passivation of a corrosion resistant high entropy alloy in non-oxidizing sulfate solutions, Acta Mater. 164 (2019) 362–376.
[90] S. Ralkhal, et al., A combined electrochemical, molecular dynamics, quantum mechanics and XPS analysis of the mild steel surface protected by a complex film composed of neodymium (III) and benzimidazole, Appl. Surf. Sci. 464 (2019) 178–194.
[91] Y. Niu, et al., Characterization and corrosion resistance study of the Fe-Cr films electrodeposited from trivalent chromium sulfate electrolyte, Mater. Res. Express 6 (12) (2019).
[92] H. Ding, et al., Tribological behavior of plant oil-based extreme pressure lubricant additive in water-ethylene glycol liquid, J. Renew. Mater. 7 (12) (2019) 1391–1401.
[93] Y. Takabatake, et al., Inhibition of anodic dissolution of steel by Sn2+ in perchloric acid solution, J. Electrochem. Soc. 166 (8) (2019) C217–C223.
[94] K. Vimal Kumar, B.V.Appa Rao, Phosphorylated xanthan gum, an environment-friendly, efficient inhibitor for mild steel corrosion in aqueous 200 ppm NaCl, Mater. Today. Proc. 15 (2019) 155–165.
[95] S. Chen, et al., Corrosion of Q235 carbon steel in seawater containing mariprofundus ferrooxydans and thalassospira sp, Front. Microbiol. 10 (MAY) (2019).
[96] J.D.L. Rocha, et al., Investigation on the relationship between the surface chemistry and the corrosion resistance of electrochemically nitrided AISI 304 stainless steel, Int. J. Corros. 2019 (2019).
[97] B. Wang, et al., Combined treatment plasma electrolytic carburizing and borocarburizing on Q235 low-carbon steel, Mater. Chem. Phys. 221 (2019) 232–238.
[98] A.K. Al-Harbi, K.M. Emran, Effect of immersion time on electrochemical and morphology of new Fe-Co metal-metal glassy alloys in acid rain, Arab. J. Chem. 12 (1) (2019) 134–141.
[99] S. Madan, et al., Enhancing corrosion stability and shelf life of nanoscale zero-valent iron via encapsulation in porous Ze-TiO2 matrix: an interface for simultaneous oxidation and adsorption of As(III), Colloids Surf. A Physicochem. Eng. Asp. 607 (2020) 125381.
[100] F. Montes, et al., Silicate ions as corrosion inhibitors for carbon steel in Chloride-Contaminated concrete pore simulating solutions, Corrosion 76 (12) (2020) 1147–1154.
[101] S. Ullah, et al., The coupling of sand with ZVI/oxidants achieved proportional and highly efficient removal of arsenic, Front. Environ. Sci. Eng. 14 (6) (2020) 94.
[102] H. Wang, et al., Study on the influence of compound rust inhibitor on corrosion of steel bars in chloride concrete by electrical parameters, Constr. Build. Mater. 262 (2020) 120763.
[103] Y.P. Sun, et al., Effects of the element la on the corrosion properties of CrMnFeNi high entropy alloys, J. Alloy. Compd. 842 (2020) 155825.
[104] G. Su, et al., New insights into the corrosion behaviour of medium manganese steel exposed to a NaCl solution spray, Constr. Build. Mater. 261 (2020) 119908.
[105] A. Berrissoul, et al., Anticorrosion effect of a Green sustainable inhibitor on mild steel in hydrochloric acid, J. Colloid Interface Sci. 580 (2020) 740–752.
[106] Z. Xu, et al., Enhanced reactivity and electron selectivity of GAC-Fe-Cu ternary micro-electrolysis system toward p-chloronitrobenzene under oxic conditions, J. Hazard. Mater. 398 (2020) 123122.
[107] C.B. Nascimento, et al., Electronic properties of the passive films formed on CoCrFeNi and CoCrFeNiAl high entropy alloys in sodium chloride solution, J. Mater. Res. Technol. 9 (6) (2020) 13879–13892.
[108] X. Yuan, et al., Natural passivation behavior and its influence on chloride-induced corrosion resistance of stainless steel in simulated concrete pore solution, J. Mater. Res. Technol. 9 (6) (2020) 12378–12390.
[109] P. Yang, et al., Improved corrosive wear resistance of carbidic austempered ductile iron by addition of cu, Mater. Charact. 168 (2020) 110577.
[110] S. Zanna, et al., Escherichia coli siderophore-induced modification of passive films on stainless steel, Corros. Sci. 175 (2020) 108872.
[111] Y. Yang, et al., Characterization, formation and development of scales on L80 steel tube resulting from seawater injection treatment, J. Pet. Sci. Eng. 193 (2020) 107433.
[112] J. Hu, Y. Liu, W. Li, Microstructure and corrosion behavior of FeCrNiMnMo high-entropy alloys fabricated by the laser surface remelting, Mater. Corros. 71 (10) (2020) 1747–1754.
[113] N.A. Khan, et al., RF magnetron sputtered AlCoCrCu0.5FeNi high entropy alloy (HEA) thin films with tuned microstructure and chemical composition, J. Alloy. Compd. 836 (2020) 155348.
[114] T. Nakagawa, et al., Corrosion behavior of SUS 304L steel in ph 13 NaOH solution, Electrochemistry 88 (5) (2020) 468–474.
[115] H. Fu, et al., Facile synthesis of Al/Fe bimetallic (oxyhydr)oxide-coated magnetite for efficient removal of fluoride from water, Environ. Technol. (U. Kingd.) 41 (20) (2020) 2625–2636.
[116] Z.-Z. Yin, et al., Self-catalytic degradation of iron-bearing chemical conversion coating on magnesium alloys — influence of fe content, Front. Mater. Sci. 14 (3) (2020) 296–313.
[117] X. Zhang, et al., Selective oxidation of ternary Fe-Mn-Si alloys during annealing process, Corros. Sci. 174 (2020) 108859.
[118 A. Espinoza-Vázquez, et al., Fluconazole and fragments as corrosion inhibitors of API 5L X52 steel immersed in 1M HCl, Corros. Sci. 174 (2020) 108853.
[119] S. Varvara, et al., Dissolution of metals in different Bromide-Based systems: electrochemical measurements and spectroscopic investigations, Materials 13 (16) (2020) 3630.
[120] S. Mandal, et al., Effect of Phosphate-Based inhibitor on corrosion kinetics and mechanism for formation of passive film onto the steel rebar in Chloride-Containing pore solution, Materials 13 (16) (2020) 3642.
[121] S. Detriche, et al., XPS fast depth profile of the native oxide layers on AISI 304, 316 and 430 commercial stainless steels and their evolution with time, J. Electron. Spectrosc. Relat. Phenom. 243 (2020) 146970.
[122] R. Babilas, et al., Relationship between the thermodynamic parameters, structure, and anticorrosion properties of Al-Zr-Ni-Fe-Y alloys: physical metallurgical and materials science, Metall. Mater. Trans. 51 (8) (2020) 4215–4227.
[123] M. Zhou, et al., Pinewood outperformed bamboo as feedstock to prepare biochar-supported zero-valent iron for Cr6+ reduction, Environ. Res. 187 (2020) 109695.
[124] A. Hassan, et al., Formation of a self-organized nanoporous structure with open-top morphology on 304L austenitic stainless steel, Nanotechnology 31 (31) (2020) 315603.
[125] J. Yang, et al., Preparation and properties of the anodized film on Fe-Cr-Al alloy surface, Anti Corros. Methods Mater. 67 (4) (2020) 379–386.
[126] G. Yang, et al., Effect of liquid flow velocity on corrosion behavior of 20# steel at initial stage under gas-liquid two-phase plug flow condition, Anti Corros. Methods Mater. 67 (4) (2020) 415–425.
[127] D. Ewis, et al., Corrosion behavior of API-X120 carbon steel alloy in a GTL F-T process water environment at low COD concentration, Metals 10 (6) (2020).
[128] K. Idczak, R. Idczak, Investigation of surface segregation in Fe-Cr-Si alloys by XPS: physical metallurgical and materials science, Metall. Mater. Trans. 51 (6) (2020) 3076–3089.
[129] P. Wongpanya, et al., Erosion–corrosion behaviors of 1045 and J55 steels in crude oil, J. Pet. Sci. Eng. 189 (2020) 106965.
[130] C. Thinaharan, R.P. George, J. Philip, In situ Raman spectroscopic analysis on carbon steel, immersed in aqueous solutions at different ph and anions, J. Mater. Eng. Perform. 29 (5) (2020) 2792–2805.
[131] L. Wang, et al., Study of the surface oxides and corrosion behaviour of an equiatomic CoCrFeMnNi high entropy alloy by XPS and ToF-SIMS, Corros. Sci. 167 (2020) 108507.
[132] L. Ma, et al., Passivation mechanisms and pre-oxidation effects on model surfaces of FeCrNi austenitic stainless steel, Corros. Sci. 167 (2020) 108483.
[133] M. Petrunin, et al., Thin benzotriazole films for inhibition of carbon steel corrosion in neutral electrolytes, Coatings 10 (4) (2020) 362.

[134] R. Chen, et al., Characterization of the passive film formed on the reinforcement surface in alkali activated Fly ash: surface analysis and electrochemical evaluation, Corros. Sci. 165 (2020) 108393.
[135] J.-L. Gu, et al., An abnormal correlation between electron work function and corrosion resistance in Ti-Zr-Be-(Ni/Fe) metallic glasses, Corros. Sci. 165 (2020) 108392.
[136] Y. Dou, et al., Characterization of the passive properties of 254SMO stainless steel in simulated desulfurized flue gas condensates by electrochemical analysis, XPS and ToF-SIMS, Corros. Sci. 165 (2020) 108405.
[137] P. Pahuja, et al., The protection mechanism offered by heterophragma adenophyllum extract against Fe-C steel dissolution at low ph: computational, statistical and electrochemical investigations, Bioelectrochemistry 132 (2020) 107400.
[138] M. Chafiq, et al., Inhibition performances of spirocyclopropane derivatives for mild steel protection in HCl, Mater. Chem. Phys. 243 (2020) 122582.
[139] Z. Wang, et al., Comparison study on the semiconductive and dissolution behaviour of 316L and alloy 625 in hydrochloric acid solution, Acta Metall. Sin. 33 (3) (2020) 403–414.
[140] H. Lgaz, et al., Exploring the potential role of pyrazoline derivatives in corrosion inhibition of mild steel in hydrochloric acid solution: insights from experimental and computational studies, Constr. Build. Mater. 233 (2020) 117320.
[141] S. Zhang, et al., Shifts in the binding energies of Cr2p, Fe2p and O1s electrons of alloy oxide films in the presence of pb during High-Temperature water corrosion, Int. J. Electrochem. Sci. 15 (2) (2020) 1853–1860.
[142] Y. Yao, et al., Corrosion protection of epoxy coatings containing 2-hydroxy-phosphonocarboxylic acid doped polyaniline nanofibers, Prog. Org. Coat. 139 (2020) 105470.
[143] H. Luo, et al., Influence of carbon on the corrosion behaviour of interstitial equiatomic CoCrFeMnNi high-entropy alloys in a chlorinated concrete solution, Corros. Sci. 163 (2020) 108287.
[144] Y.S. Lu, et al., Corrosion behavior and passive film characterization of Fe50Mn30Co10Cr10 Dual-Phase High-Entropy alloy in sulfuric acid solution, J. Electrochem. Soc. 167 (8) (2020).
[145] I.N. Shabanova, et al., XPS investigation of adsorption protective layers based on industrial inhibited oil, Int. J. Corros. Scale Inhib. 9 (3) (2020) 903–911.
[146] S.M. Reshetnikov, et al., Effect of laser treatment of unalloyed steel on the efficiency of benzotriazole as a corrosion inhibitor in a neutral medium, Int. J. Corros. Scale Inhib. 9 (3) (2020) 1113–1120.
[147] W. Liu, et al., Revealing the enhanced passivation and Anti-Corrosion performance of Surface-Nanocrystallization-Modified Cr-Alloyed rebar via electrochemical testing and XPS depth analysis, Coatings 13 (2023), https://doi.org/10.3390/coatings13010192.
[148] F. Dou, et al., Exploration of novel polyaspartic acid derivatives as fluorescent eco-friendly corrosion inhibitors for the carbon steel: electrochemical, surface analysis (SEM/XPS) and theoretical calculation, Colloids Surf. A Physicochem. Eng. Asp. 658 (2023) 130606.
[149] L. Gong, et al., Understanding of selective oxidation of Fe-Mn binary alloys during continuous annealing through X-ray photoelectron spectroscopy, Corros. Commun. 11 (2023) 72–82.
[150] S. Lu, et al., A novel biodegradable high nitrogen iron alloy with simultaneous enhancement of corrosion rate and local corrosion resistance, J. Mater. Sci. Technol. 152 (2023) 94–99.
[151] S.K. Saha, et al., Passivity of iron surface in curing cement paste environment investigated by electrochemical impedance spectroscopy and surface characterization techniques, Surf. Interfaces 36 (2023) 102549.
[152] M. Moshtaghi, et al., The effect of HPAM polymer for enhanced oil recovery on corrosion behaviour of a carbon steel and interaction with the inhibitor under simulated brine conditions, Corros. Sci. 217 (2023) 111118.
[153] Q. Gong, et al., Corrosion of pipeline steel weld metals containing alloying elements in CO2/H2S environment, Gas. Sci. Eng. 109 (2023) 104846.
[154] P. Kesari, et al., Chitosan based titanium and iron oxide hybrid bio-polymeric nanocomposites as potential corrosion inhibitor for mild steel in acidic medium, Int. J. Biol. Macromol. 225 (2023) 1323–1349.
[155] K. Subbiah, et al., Assessment of the inhibitive performance of a hydrazone derivative for steel rebar in a simulated concrete medium: establishing the inhibition mechanism at an experimental and theoretical level, Chem. Eng. J. 458 (2023) 141347.
[156] Q. Xu, et al., Enhanced corrosion resistance of laser additive manufactured 316L stainless steel by ultrasonic surface rolling process, Surf. Coat. Technol. 454 (2023) 129187.
[157] Y. Li, et al., Effect of cooling rate on segregation characteristics of 254SMO super austenitic stainless steel and pitting corrosion resistance under simulated flue gas desulfurization environment, J. Mater. Sci. 58 (9) (2023) 4137–4149.
[158] X. Li, X. Xin, S. Deng, Synergism between walnut Green husk extract and sodium dodecyl benzene sulfonate on cold rolled steel in 1.0 mol/l H2SO4 solution, Corros. Commun. 9 (2023) 1–12.
[159] M. Tang, et al., Mikania micrantha extract/KI blend as a novel synergistic inhibitor for steel corrosion in concentrated H3PO4 solution, Ind. Crops Prod. 193 (2023) 116237.
[160] M. Ouyang, et al., Corrosion behaviour of super ferritic stainless steel 020Cr25MoCuNbTi in the waste phosphoric acid of a surface treatment process, Corros. Sci. 212 (2023) 110921.
[161] Q. Gao, et al., Effect of oil displacement agent on corrosion behavior of NaCl - alkali/ surfactant/ polymer flooding pipeline steel, Vacuum 209 (2023) 111742.
[162] R. Qi, et al., Controlling the thickness and composition of stainless steel surface oxide film for anodic sulfide removal, J. Clean. Prod. 389 (2023) 136076.
[163] T. Xiang, et al., Synergistic inhibition of benzotriazole and sodium D-gluconate on steel corrosion in simulated concrete pore solution, Colloids Surf. A Physicochem. Eng. Asp. 661 (2023) 130918.
[164] A. Collazo, et al., Electrochemical characterization of a Fe-based shape memory alloy in an alkaline medium and the behaviour in aggressive conditions, Electrochim. Acta 444 (2023) 142034.
[165] T.A. Yousef, et al., Experimental and theoretical examinations of triazole linked saccharin derivatives as organic corrosion inhibitors for mild steel in hydrochloric acid, J. Mol. Struct. 1275 (2023) 134603.
[166] W. Yan, et al., Localized corrosion mechanism of Q125 casing steel in residual acid solution during oil reservoir acidizing, Coatings 13 (2023), https://doi.org/10.3390/coatings13040710.
[167] S.A. Policastro, R.M. Anderson, C.M. Hangarter, Modeling and predicting reduction reaction kinetics for a Stainless-Steel in NaCl solutions, J. Electrochem. Soc. 170 (4) (2023) 041504.
[168] S. Habib, et al., Polymeric smart coatings containing modified capped halloysite nanotubes for corrosion protection of carbon steel, J. Mater. Sci. 58 (15) (2023) 6803–6822.
[169] B. Lin, et al., Passiflora edulis sims peel extract as a renewable corrosion inhibitor for mild steel in phosphoric acid solution, J. Mol. Liq. 375 (2023) 121296.
[170] W. Emori, et al., Dispersive adsorption and anticorrosion properties of natural capsaicin on Q235 steel in mixed H2SO4 and NaCl environment: characterization, experimental and theoretical studies, Sustain. Chem. Pharm. 32 (2023) 101042.
[171] A. Singh, et al., Evaluation of corrosion mitigation properties of pyridinium-based ionic liquids on carbon steel in 15% HCl under the hydrodynamic condition: experimental, surface, and computational approaches, J. Mol. Liq. 376 (2023) 121408.
[172] L. Yan, et al., Passivation effect of the chlorinated paraffin added in the cutting fluid on the surface corrosion resistance of the stainless steel, Molecules 28 (2023), https://doi.org/10.3390/molecules28093648.
[173] C. Liu, S. Wei, S. Lu, Corrosion behavior of 9Cr-Si heat resistant steel deposited metal in liquid lead-bismuth eutectic at 550 °, C. Corros. Sci. 215 (2023) 111042.
[174] J.D. Choundraj, et al., Influence of native oxide film on corrosion behavior of additively manufactured stainless steel 316, L. Corros. Sci. 217 (2023) 111098.
[175] L. Huang, H.-J. Li, Y.-C. Wu, Comprehensive evaluation of corrosion inhibition performance and ecotoxicological effect of cinchona IIa as a Green corrosion inhibitor for pickling of Q235 steel, J. Environ. Manag. 335 (2023) 117531.
[176] X. Wang, et al., XPS study of the thermal stability of passivated NiCrFeCoMo multi-principal element alloy surfaces, Surf. Interface Anal. 55 (6-7) (2023) 457–465.
[177] N.M. El-Basiony, et al., Theoretical and experimental insights into the C-steel aqueous corrosion inhibition at elevated temperatures in 1.0 M HCl via multi-carbonyl gemini cationic surfactants 237 (6) (2023) 707–736.
[178] R.K. Mehta, S.K. Gupta, M. Yadav, Synthesized novel carbon dots as Green corrosion inhibitor for mild steel in hydrochloric acid: gravimetric, electrochemical and morphological studies, Diam. Relat. Mater. 136 (2023) 109992.
[179] B. Liao, et al., Fructus cannabis protein extract powder as a Green and high effective corrosion inhibitor for Q235 carbon steel in 1 m HCl solution, Int. J. Biol. Macromol. 239 (2023) 124358.
[180] P. Kesari, et al., Biopolymer sodium alginate based titania and magnetite nanocomposites as natural corrosion inhibitors for mild steel in acidic medium, J. Ind. Eng. Chem. 122 (2023) 303–325.
[181] Y.G. Avdeev, et al., Thin 1,2,4-Triazole films for the inhibition of carbon steel corrosion in sulfuric acid solution, Coatings 13 (2023), https://doi.org/10.3390/coatings13071221.
[182] D. Bonfil, et al., Corrosion activity of stainless steel SS430 and carbon steel B450C in a sodium silicate modified Limestone-Portland cement extract, Materials 16 (2023), https://doi.org/10.3390/ma16145066.
[183] Z. Geng, et al., Understanding the intrinsic effect of Fly ash on passivity and chloride-induced corrosion of carbon steel and stainless steel in cement extract solutions, Cem. Concr. Compos. 143 (2023) 105236.
[184] L. Wang, et al., Adsorption mechanism of quaternary ammonium corrosion inhibitor on carbon steel surface using ToF-SIMS and XPS, Corros. Sci. 213 (2023) 110952.
[185] N.B. Iroha, et al., Linagliptin drug molecule as corrosion inhibitor for mild steel in 1 m HCl solution: electrochemical, SEM/XPS, DFT and MC/MD simulation approach, Colloids Surf. A Physicochem. Eng. Asp. 660 (2023) 130885.
[186] X. Jiang, et al., Corrosion behavior of fluorinated carbonyl iron-hydrophobic composites in neutral salt spray environment, Corros. Sci. 210 (2023) 110823.
[187] T. Cui, et al., Towards understanding shewanella algae-induced degradation of passive film of stainless steel based on electrochemical, XPS and multi-mode AFM analyses, Corros. Sci. 218 (2023) 111174.
[188] J. Haque, et al., Environmentally benign Water-Soluble sodium L-2-(1-Imidazolyl) alkanoic acids as new corrosion inhibitors for mild steel in artificial seawater, ACS Omega 8 (28) (2023) 24797–24812.
[189] O. Kharbouch, et al., Enhancing corrosion resistance of mild steel in 1M HCl: investigation of new benzoxazepine derivatives through synthesis, electrochemical analysis, surface analysis, XPS, DFT, and molecular dynamics simulation, ChemistrySelect 9 (15) (2024) e202303045.
[190] X. Wang, et al., Mechanism for corrosion inhibition of pure iron in 1 m HCl by rauiella fujisana: experimental, GCMS, DFT, VASP and solidliquid modeling studies, Ind. Crops Prod. 207 (2024) 117692.
[191] S. Polić, et al., Corroded medieval iron nail from the studenica monastery - material analysis and laser cleaning, J. Cult. Herit. 66 (2024) 367–374.

[192] O. Safdarzadeh, et al., WLI, XPS and SEM/FIB/EDS surface characterization of an electrically fluted bearing raceway, Lubricants 12 (2024), https://doi.org/10.3390/lubricants12050148.
[193] Y. Jin, et al., Effect of exogenous flavins on the microbial corrosion by geobacter sulfurreducens via iron-to-microbe electron transfer, J. Mater. Sci. Technol. 171 (2024) 129–138.
[194] W. Liu, et al., Effect of heat treatment on the corrosion resistance of 316L stainless steel manufactured by laser powder bed fusion, J. Mater. Res. Technol. 32 (2024) 3896–3912.
[195] Z. Song, et al., Inhibition performance of extract reinforcement corrosion inhibitor from waste platanus acerifolia leaves in simulated concrete pore solution, Case Stud. Constr. Mater. 20 (2024) e02992.
[196] Y. Chen, et al., Synergistic effects of trace sulfadiazine and corrosion scales on disinfection by-product formation in bulk water of cast iron pipe, Environ. Pollut. 341 (2024) 122866.
[197] H. Shao, et al., Sulfur dots corrosion inhibitors with superior antibacterial and fluorescent properties, J. Colloid Interface Sci. 654 (2024) 878–894.
[198] A.E.-A.S. Fouda, et al., Verbena officinalis (VO) leaf extract as an anti-corrosion inhibitor for carbon steel in acidic environment, Sci. Rep. 14 (1) (2024) 16112.
[199] B. Martínez-Aparicio, et al., Evaluation of passive films on 17-7PH and 410 stainless steel exposed to NaCl solution, Materials 17 (2024), https://doi.org/10.3390/ma17164060.
[200] D. Narayanan, et al., Localized corrosion in selective laser melted SS316L in CO2 and H2S brines at elevated temperatures, npj Mater. Degrad. 8 (1) (2024) 50.
[201] P. Du, et al., Synergistic inhibition of mikania micrantha extract with iodide ion on the corrosion of cold rolled steel in trichloroacetic acid medium, J. Ind. Eng. Chem. 139 (2024) 358–377.
[202] A. Suhasaria, et al., Electrochemical behavior of mild steel coated with long alkyl-chain benzothiazole derivatives in acid solution: effect of aliphatic chain length, Colloids Surf. A Physicochem. Eng. Asp. 703 (2024) 135264.
[203] Q. Fu, et al., Depassivation mechanism of steel bar in concrete under the condition of flowing composite chloride salt and sulfate attack, Constr. Build. Mater. 450 (2024) 138696.
[204] Q. Wang, et al., Seaweed extract as Green corrosion inhibitor for carbon steel in hydrochloric acid solution, Colloids Surf. A Physicochem. Eng. Asp. 700 (2024) 134751.
[205] S. Shao, M. Guo, Y. Zhang, Natural passivation and chloride corrosion resistance of inconel 625 in OPC and CSA concrete pore solutions with different ph, Cem. Concr. Compos. 154 (2024) 105794.
[206] S. Chen, et al., Solanum tuberosum leaf extract as an eco-friendly corrosion inhibitor for Q235-steel in HCl medium: experimental and theoretical evaluation, Int. J. Electrochem. Sci. 19 (11) (2024) 100818.
[207] Q. Wang, et al., Study on the corrosion inhibitory performance of pomacea canaliculata extract as a corrosion inhibitor for carbon steel in acidic environments, J. Mol. Liq. 394 (2024) 123754.
[208] Y. Wang, et al., Novel chitosan-oligosaccharide derivatives as fluorescent Green corrosion inhibitors for P110 steel, Carbohydr. Polym. 343 (2024) 122475.
[209] B. Gu, et al., Effect of ultrasonic impact treatment on surface residual stress, microstructure and electrochemical properties of the hot-rolled S355 steel, Surf. Coat. Technol. 494 (2024) 131468.
[210] L.K.M.O. Goni, et al., Synthesis of a new quaternary ammonium salt for efficient inhibition of mild steel corrosion in 15% HCl: experimental and theoretical studies, Heliyon 10 (19) (2024) e38425.
[211] L. Matějovský, et al., Amines as steel corrosion inhibitors in ethanol-gasoline blends, Fuel 361 (2024) 130681.
[212] L. Matějovský, et al., The use of amines as steel corrosion inhibitors in butanol-gasoline blends, Fuel 374 (2024) 132413.
[213] H. Wang, et al., Influence of carboxymethyl chitosan and sodium humate composite corrosion inhibitor on the corrosion resistance of EH40 steel in seawater, Langmuir 40 (40) (2024) 21263–21279.
[214] H. Yang, S. Deng, X. Li, Eupatorium adenophorum spreng root extract as an efficient inhibitor for the corrosion of steel in sulfamic acid solution, Int. J. Electrochem. Sci. 19 (10) (2024) 100790.
[215] S. Nie, et al., Corrosion behavior of as-cast Al0.75CoCr1.25FeNi high entropy alloy in 0.5 mol/l sulfuric acid, Adv. Compos. Hybrid. Mater. 7 (5) (2024) 138.
[216] A. Belkheiri, et al., In-depth study of a newly synthesized imidazole derivative as an eco-friendly corrosion inhibitor for mild steel in 1 M HCl: theoretical, electrochemical, and surface analysis perspectives, Int. J. Electrochem. Sci. 19 (10) (2024) 100768.
[217] L. Qiu, et al., Comparison of the corrosion inhibition property on cold rolled steel in sulfuric acid media between reflux and ultrasound extracts from rapeseed meal, Ind. Crops Prod. 216 (2024) 118809.
[218] Q. Sun, et al., Isoindigo derivatives as some potential corrosion inhibitors for mild steel in hydrochloric acid solution: synthesis, experimental and theoretical studies, J. Mol. Struct. 1312 (2024) 138480.
[219] M.A. Chidiebere, V.C. Anadebe, R.C. Barik, Insight into the corrosion resistance of mild steel in an acidic environment in the presence of an organic extract: experimental and computational approach, Results Eng. 23 (2024) 102787.
[220] C. Zeng, et al., Exploration on the corrosion inhibition performance of salvia miltiorrhiza extract as a Green corrosion inhibitor for Q235 steel in HCl environment, J. Mater. Res. Technol. 32 (2024) 3857–3870.
[221] S. Wang, et al., Humic acid as eco-friendly corrosion inhibitor for EH40 ship plate steel, Surf. Interface Anal. 56 (9) (2024) 654–665.
[222] X. Luo, et al., Zwitterion modified chitosan as a high-performance corrosion inhibitor for mild steel in hydrochloric acid solution, Int. J. Biol. Macromol. 267 (2024) 131429.
[223] M. Marczewski, W. Tylus, J. Winiarski, The effect of anodic polarization parameters of 316L steel in a propylene glycol: choline chloride eutectic solvent on surface finishing, chemistry and corrosion resistance, Appl. Surf. Sci. 652 (2024) 159335.
[224] N. Timoudan, et al., Investigation of the mechanisms and adsorption of a new pyrazole derivative against corrosion of carbon steel in hydrochloric acid solution: experimental methods and theoretical calculations, Colloids Surf. A Physicochem. Eng. Asp. 682 (2024) 132771.
[225] A.C. Njoku, et al., Anticorrosion performance of nicotinic acid and nicotinic acid hydrazide blended with optimized potassium iodide against Q235 steel corrosion in acid-chloride medium, J. Mol. Struct. 1297 (2024) 136861.
[226] E.L. Maia, et al., Early stages of liquid-metal corrosion on pre-oxidized surfaces of austenitic stainless steel 316L exposed to static Pb-Bi eutectic at 400 °, C. Corros. Sci. 227 (2024) 111680.
[227] A. Singh, et al., Long chain imidazole derivative as a novel corrosion inhibitor for Q235 steel in 15% HCl medium under hydrodynamic condition: experimental and theoretical examinations, Mater. Chem. Phys. 313 (2024) 128798.
[228] B. Tamilselvi, et al., Investigation of corrosion inhibition of mild steel in 0.5 m H2SO4 with lachancea fermentati inhibitor extracted from rotten grapefruits (Vitis vinifera): adsorption, thermodynamic, electrochemical, and quantum chemical studies, ACS Phys. Chem. Au 4 (1) (2024) 67–84.
[229] L. Cui, et al., Benzothiazole-based ionic liquids as environment-friendly and high-efficiency corrosion inhibitors for mild steel in HCl: experimental and theoretical studies, J. Mol. Liq. 394 (2024) 123769.
[230] R. Yıldız, et al., Corrosion behavior of mild steel in 1 m HCl with cyclotrichium niveum as a Green inhibitor, Mater. Chem. Phys. 312 (2024) 128654.
[231] M. O.A. Ferreira, et al., Niobium and carbon nanostructured coatings for corrosion protection of the 316L stainless steel, Mater. Chem. Phys. 312 (2024) 128610.
[232] K. Dahmani, et al., Evaluating the efficacy of synthesized quinoline derivatives as corrosion inhibitors for mild steel in acidic environments: an analysis using electrochemical, computational, and surface techniques, J. Mol. Struct. 1295 (2024) 136514.
[233] J.P. Aguilar-Barrientos, M.A. Pech-Canul, M.A. Fernández-Herrera, Corrosion inhibition of carbon steel in neutral chloride solutions using salts of primary bile acids, ACS Omega 9 (39) (2024) 40980–40991.
[234] M. Galai, et al., Surface analysis and interface properties of a newly synthesized quinoline-derivative corrosion inhibitor for mild steel in acid pickling bath: mechanistic exploration through electrochemical, XPS, AFM, contact angle, SEM/EDS, and computational studies, J. Phys. Chem. Solids 184 (2024) 111681.
[235] N. Timoudan, et al., Enhanced corrosion resistance of carbon steel in an aggressive environment by a recently developed pyrazole derivative: electrochemical, SEM/XPS/AFM, and theoretical investigation, J. Solid State Electrochem. 28 (8) (2024) 2837–2860.
[236] S. Kohiki, K. Oki, An appraisal of evaporated gold as an energy reference in X-ray photoelectron spectroscopy, J. Electron Spectrosc. Relat. Phenom. 36 (1) (1985) 105–110.
[237] A.E. Hughes, B.A. Sexton, Comments on the use of implanted ar as a binding energy reference, J. Electron Spectrosc. Relat. Phenom. 50 (2) (1990) C15–C18.
[238] B.M. Clark, et al., Following the propagation of erroneous x-ray photoelectron spectroscopy peak fitting through the literature. A genealogical approach, J. Vac. Sci. Technol. A Vac. Surf. Films 42 (6) (2024).
[239] G.H. Major, et al., Perspective on improving the quality of surface and material data analysis in the scientific literature with a focus on x-ray photoelectron spectroscopy (XPS), J. Vac. Sci. Technol. A Vac. Surf. Films 41 (3) (2023).
[240] M.C. Biesinger, Accessing the robustness of adventitious carbon for charge referencing (correction) purposes in XPS analysis: insights from a multi-user facility data review, Appl. Surf. Sci. 597 (2022) 153681.
[241] D.R. Baer, et al., XPS guide: charge neutralization and binding energy referencing for insulating samples, J. Vac. Sci. Technol. A 38 (3) (2020) 031204.
[242] M.A. El-Hashemy, et al., Electrochemical and surface characterisation of carbon steel exposed to mixed ce and iodide electrolytes, Metals 13 (9) (2023).
[243] E. Li, et al., Choline amino acid ionic liquids as Green corrosion inhibitors of mild steel in acidic medium, Colloids Surf. A Physicochem. Eng. Asp. 657 (2023) 130541.
[244] Q. Wang, et al., Synergistic effect of KI on corrosion inhibition of carbon steel by styphnolobium japonicum (L.) schott in H2SO4 solution, J. Mol. Struct. 1309 (2024) 138251.
[245] G.H. Major, et al., Insufficient reporting of x-ray photoelectron spectroscopy instrumental and peak fitting parameters (metadata) in the scientific literature, J. Vac. Sci. Technol. A Vac. Surf. Films 41 (4) (2023).
[246] D.J. Blackwood, et al., Macrofouling induced localized corrosion of stainless steel in Singapore seawater, Corros. Sci. 129 (2017) 152–160.
[247] Z. Qi, et al., Enhanced oxidative and adsorptive capability towards antimony by copper-doping into magnetite magnetic particles, RSC Adv. 6 (71) (2016) 66990–67001.
[248] P. Refait, et al., Localized corrosion of carbon steel in marine media: galvanic coupling and heterogeneity of the corrosion product layer, Corros. Sci. 111 (2016) 583–595.
[249] M. Razmjoo Khollari, et al., Comprehensive analysis of alloy 800 corrosion using Thermo-Kinetic diagrams, Corros. Sci. 253 (2025) 112967 (-undefined).

[250] N. Pauly, et al., XPS primary excitation spectra of zn 2p, fe 2p, and ce 3d from ZnO, α-Fe2O3, and CeO2, Surf. Interface Anal. 51 (3) (2019) 353–360.
[251] S. Tougaard, Inelastic background correction and quantitative surface analysis, J. Electron. Spectrosc. Relat. Phenom. 52 (1990) 243–271.
[252] P.S. Bagus, et al., Origin of the complex main and satellite features in fe 2p XPS of Fe2O3, Phys. Chem. Chem. Phys. 24 (7) (2022) 4562–4575.